Effect of environmental data uncertainty in the framework of second generation intact stability criteria

Gabriele Bulian [a,*], Andrea Orlandi [b]

[a] Department of Engineering and Architecture, University of Trieste, Via A.Valerio 10, 34127, Trieste, Italy
[b] Consorzio LaMMA, c/o CNR-IBE, Florence Research Area, Via Madonna del Piano n.10, Edificio D, 50019, Sesto Fiorentino, FI, Italy

ARTICLE INFO

Keywords:
Second generation intact stability criteria
Operational limitations
Environmental conditions
Uncertainty
Parametric roll
Mediterranean Sea

ABSTRACT

The framework of second generation intact stability criteria in MSC.1/Circ.1627 includes a number of novelties for intact stability assessment. One of such novelties is the inherent possibility of designing a vessel for a specific operational area, by embedding area-specific environmental conditions. This is practically achieved through modification of the relevant calculation parameters in the criteria, on the basis of available MetOcean data. However, MetOcean data for a given area are generally available from multiple sources, and different sources provide information on environmental conditions on the basis of different approaches. This leads to a source-related variability that eventually reflects in the results of stability assessment, to an extent that is yet to be fully explored. The present study aims at providing quantitative indications in this respect. The Mediterranean Sea is considered as operational area, five different sources of MetOcean data are used, and level 1 and level 2-check 1 vulnerability criteria for parametric rolling are applied to two sample ships. The variability in the obtained safe zones of loading conditions is presented and discussed, also with reference to the effect of bilge keels. Some difficulties in the practical implementation of the procedure for embedding operational limitations are also highlighted and discussed.

1. Introduction

After many years of development, the Interim Guidelines on the Second Generation Intact Stability Criteria (SGISC) have been approved by the IMO Maritime Safety Committee as MSC.1/Circ.1627 (IMO, 2020) at the end of 2019. The Interim Guidelines contain the application framework of the second generation intact stability criteria, and are complemented by the corresponding Explanatory Notes, which, at the moment of writing, are at an advanced stage of development (IMO, 2021b).

From a general perspective, the framework of SGISC opens the door to the application of new approaches for intact stability assessment, focussing on ship dynamics. The framework considers multiple failure modes, namely dead ship condition, excessive acceleration, pure loss of stability, parametric rolling and surf-riding/broaching. Each failure mode can be addressed with different levels of assessment of increasing complexity and correspondingly expected accuracy.

One of the important characteristics of the framework of SGISC is the possibility of implementing so-called "operational measures", in the form of "operational limitations" or "operational guidance". The possibility of implementing operational measures is a consequence of the recognition in MSC.1/Circ.1627 (IMO, 2020) that "an integrated perspective, combining design methods and operational measures, is the most effective way for properly addressing and continuously improving safety against accidents related to stability for ships in a seaway".

One of the possible operational measures is the design of the vessel for a specific area of operation, by implementing operational limitations. In fact, area-specific environmental conditions can be embedded in some of the SGISC through a corresponding modification of the calculation parameters, according to procedures that are specified by the Explanatory Notes (IMO, 2021b). Operational limitations can also be implemented for a specific operational area considering specific routes and, if appropriate, seasons. Furthermore, operational limitations can also be implemented considering a limitation on the maximum significant wave height permitted in operation.

As a result, environmental data for the chosen ship operational area can substitute the reference environmental conditions of the SGISC, which correspond to those of North Atlantic according to IACS Rec. 34 (IACS, 2001).

The possibility of modifying the reference environmental conditions

* Corresponding author.
E-mail addresses: gbulian@units.it (G. Bulian), orlandi@lamma.toscana.it (A. Orlandi).

Accepted 3 April 2022

used in the calculations is a significant step forward compared to intact stability regulations in the 2008 IS Code (IMO, 2021a), as this provides additional degrees of freedom to the designer.

This novelty indeed already attracted attention in the past regarding its potential effects on design and operation, and the attention on this topic has significantly grown very recently, following the finalization of MSC.1/Circ.1627 (IMO, 2020).

Sasdelli (2015) assessed the effect of the introduction of operational limitations for a containership, with reference to parametric roll level 1 and level 2-check 1 assessment, considering Mediterranean Sea and North Sea. Clear variations in the regions of acceptable loading conditions were identified depending on the selected area or the use of environmental data for unrestricted service. Bačkalov et al. (2016) discussed on challenges and opportunities, and potential benefits and shortcomings of an integrated approach to intact stability, combining design and operational risk control options. The topic was addressed from a wide general perspective and, in the discussion, the uncertainty in environmental data was mentioned with reference to weather forecasts. Hashimoto et al. (2017) investigated the effect of the introduction of constraints based on parametric roll level 2 assessment, with reference to actual navigation. To this end, a navigation simulation model developed for weather routing was used, considering a containership. However, based on the framework in MSC.1/Circ.1627 (IMO, 2020), the approach followed by Hashimoto et al. (2017) should be categorised as a level 2-based operational guidance, rather than an implementation of operational limitation. Rudaković and Bačkalov (2019) borrowed the approaches that are presently embedded in MSC.1/Circ.1627 (IMO, 2020) and which are generally applicable to seagoing ships, for actual application to river-sea ships. In fact, the specific operation of river-sea ships may significantly benefit from a tailored consideration of environmental conditions, since these ships, which are primarily operated in inland waters, make short trips also in coastal regions. The analysis considered level 2 vulnerability assessment for dead-ship condition and excessive accelerations, implementing variations of environmental conditions, and allowed to identify the most effective design measures to improve the operational domain of the considered ship. Rinauro et al. (2020) considered operational limitations in case of surf-riding/broaching failure mode for a fast ship. The vessel was considered to be sailing in the Mediterranean Sea, therefore, area-specific environmental conditions were considered in the level 2 assessment. In addition, limitations on the maximum significant wave height were also explored, as well as simplified operational guidance. Results indicated significant extension of the maximum operational speed when the operation was limited to the Mediterranean Sea, and these effects further increased when limitations were introduced also in terms of maximum permitted operational significant wave height. Petacco and Gualeni (2020) provided an example application to a Ro-Ro pax ferry of level 1 and level 2 criteria for pure loss of stability, dead ship condition and excessive acceleration, considering unrestricted operation, operation with limitation to given maximum significant wave height, and operational limitation in the area of Mediterranean Sea. Results of calculations indicated a limited effect of operational limitations on the dead ship condition assessment. Petacco and Gualeni (2021) carried out a subsequent study along the same line, where operational limitations and simplified operation guidance were both on focus, considering parametric roll, pure loss of stability and excessive acceleration, for a mega yacht and a Ro-Ro ferry. Paroka et al. (2021) investigated operational limitations for an Indonesian Ro-Ro ferry, considering the excessive acceleration failure mode and specific environmental data relevant to navigation in Indonesia. Hashimoto and Furusho (2021) investigated the practicability of implementing operational limitations for a C11 class containership and a PCTC, taking into account the parametric rolling failure mode. Operational limitations related to maximum significant wave height and to areas or route and season were considered, using environmental data from Global Wave Statistics (BMT, 2021). To identify relevant geographical areas for the development of a representative wave scatter table, Hashimoto and Furusho (2021) took into account ship traffic based on AIS data, and considered four different routes/areas, namely North Atlantic route, North Pacific route, East South China Sea, Mediterranean Sea. The effect of seasonality was also investigated. Bulian and Francescutto (2021) investigated the possibility of developing a simple rational procedure for embedding operational limitations in the level 1 assessment for the dead ship failure mode. The work by Bulian and Francescutto (2021) was stimulated by the fact that, according to MSC.1/Circ.1627 (IMO, 2020), the implementation of operational limitations for level 1 assessment for dead ship condition is possible in principle, but the framework is missing a corresponding calculation procedure. Shigunov et al. (2021) carried out a review of research related to intact stability in operation, both within and outside the framework of MSC.1/Circ.1627 (IMO, 2020). In the discussion of issues related to the preparation and implementation of operational measures, Shigunov et al. (2021) recalled the issue of uncertainty in weather forecasts previously pointed out by Bačkalov et al. (2016).

As can be noticed from the reported literature survey, the majority of the application cases focused on assessing the effect of implementation of operational limitations, i.e. modified MetOcean conditions, on the design and/or operation of the ship. However, environmental data for a given operational area are generally available from multiple sources, and different sources provide information on environmental conditions on the basis of different approaches. Eventually, this leads to a general source-related variability of environmental data. This variability can be considered to be due to the combination of two types of uncertainty: an epistemic and an aleatory uncertainty. The aleatory uncertainty can be linked, in the frame of the present study, to the effect of statistical analysis of a necessarily limited set of sample environmental data. The epistemic uncertainty can be linked, in the frame of the present study, to the type of used data, the type of implemented mathematical models, the process of analysis, etc., i.e., generally speaking, to "modelling". The implementation of operational limitations makes use of long-term wave statistics, which are generally derived from large datasets. Therefore, for the purpose of the present study, the inherent aleatory uncertainty may be considered to play a secondary role, and it can be expected that epistemic ("modelling") uncertainty may represent the major source of variability. However, it is important to underline that, while the separation of types of uncertainty has merits from a discussion and development perspective, from a practical application perspective, i.e. for the end user, the two types of uncertainties in the used MetOcean data are inevitably mixed.

The practical consequence of the variability of MetOcean data among different sources is that, when area-specific environmental data are embedded in the ship stability assessment process, different results can be obtained depending on the used source.

Measurement and numerical modelling techniques for MetOcean data keep on evolving, also thanks to the continuous increase in geophysical dynamics knowledge and computing power available for simulation and data processing. Overviews of the state-of-the-art related to wind and wave modelling have been provided by, e.g., Cavaleri et al. (2007, 2020) and Bhaskaran (2019). In this context, the topic of uncertainty in MetOcean data is extensively addressed in the relevant literature through validation of and comparisons among different numerical models (e.g. Stopa et al., 2016; Baordo et al., 2020). The topic of uncertainty associated with different modelling in hindcast data has also been addressed by Bitner-Gregersen et al. (2014), while discussing more generally the uncertainties associated with the description of wind and waves for engineering applications. In particular, Bitner-Gregersen et al. (2014) recognised that, despite continuous further development, different sources of MetOcean data do provide, and will keep on providing, different predictions. Indeed, recent studies addressing vessel response prediction and fatigue damage estimation (Schirmann et al., 2020) indicate that non-negligible differences can arise due to different sources of MetOcean data, and this also confirms similar results obtained

in the past (see, e.g., Guedes Soares (1999) and references therein). A further, subtle, cause of potentially non-negligible variability may also be associated with different algorithmic approaches adopted to treat the spatial dependence of MetOcean data, as investigated by Nielsen (2021). At the same time, recent studies (Campos and Guedes Soares, 2016; de Hauteclocque et al., 2020) indicate that hindcast MetOcean data from different sources are characterised by an increasing level of relative agreement, although non-negligible differences are still observed in extreme conditions. Nowadays, uncertainty in weather forecasts is also very often assessed through so-called ensemble forecasting techniques, in order to provide a quantification of uncertainty associated with initial conditions and/or modelling (e.g. Kalnay, 2003). Ensemble techniques are also used in the prediction of MetOcean conditions, where atmospheric and wave models are coupled (e.g. Saetra and Bidlot, 2002; Cao et al., 2009; Milliff et al., 2011; Pinardi et al., 2011; Meucci et al., 2018; Osinski and Radtke, 2020). Furthermore, the uncertainty associated with forecasted environmental conditions is receiving attention also in the context of weather routing of ships (e.g. Hoffschildt et al., 1999; Hinnenthal and Clauss, 2010; Mezaoui et al., 2012; Chu et al., 2015; Orlandi et al., 2015; Skoglund et al., 2015; Manderbacka, 2019; Kuhlemann and Tierney, 2020; Vettor et al., 2020). With reference to weather routing of ships it is worth noting that there are also examples in literature where ship route selection was based on combined consideration of energy efficiency and possible inception of parametric rolling (e.g. Maki et al., 2011; Park and Kim, 2015; Krata and Szlapczynska, 2018; Szlapczynska and Szlapczynski, 2019).

However, there seems to be a lack of specific studies addressing the extent to which MetOcean data variability may affect the results of stability assessment in the framework of SGISC.

The reported background and considerations have been the starting point for undertaking the study presented in this paper, which extends the initial preliminary presentation by Bulian and Orlandi (2021). In this study, a sample ship representative of a RoPax ship has been considered as main example case, using the Mediterranean Sea as reference operational area. Environmental data for the selected operational area have been gathered from five different sources. Safe zones of loading conditions have been determined using level 1 (PR-L1) and level 2 check 1 (PR-L2-C1) vulnerability criteria for parametric rolling according to MSC.1/Circ.1627 (IMO, 2020), embedding operational limitations on the basis of MetOcean data from each source. Furthermore, the effect of the presence of bilge keels has also been explicitly addressed.

The same investigation has been undertaken also for an additional ship, specifically the CEHIPAR2792 (Bulian et al., 2009, 2010). The scope of the calculations for CEHIPAR27292 is to provide an additional example application which also allows reproducibility. In fact, the geometry of the CEHIPAR2792 is publicly available.

The paper is organised as follows. Section 2 provides a summary of parametric rolling PR-L1 and PR-L2-C1 vulnerability assessment criteria, and summarises how operational limitations can be embedded in the calculations. Then, the main example application for the RoPax sample ship is provided in section 3. Section 3.1 provides a description of the main characteristics of the ship. Then, section 3.2 focusses on the environmental data and on the derived calculation parameters. The used sources of environmental data are described, and the results of the processing of the data, i.e. the wave steepness factor for PR-L1 assessment and the wave cases for PR-L2-C1 assessment, are reported. The results obtained from the different sources are also compared and discussed. Section 3.3 reports the results of the application of PR-L1 and PR-L2-C1 criteria using the calculation parameters obtained from the different sources of environmental data. For the sake of reference and completeness, results based on environmental conditions for unrestricted service are also reported. Some additional considerations regarding the performed application are then reported in section 3.4. For the second example application using the CEHIPAR2792 hull form, results are reported in the Appendix. Some concluding remarks are finally provided at the end of the paper.

2. Parametric roll vulnerability assessment and operational limitations

In this study, PR-L1 and PR-L2-C1 vulnerability criteria for parametric rolling will be used to determine safe zones of loading conditions for the considered sample ship. Details of the calculation methods are provided in section 2.5 of MSC.1/Circ.1627 (IMO, 2020), and they are briefly summarised hereinafter.

In the PR-L1 criterion, an approximate variation of metacentric height in waves, δGM_1, is calculated with a simplified method using the moments of inertia of two flat waterplanes at two draughts, above and below the actual calculation draught. The simplified method is intended to provide a conservative estimation of the variation of GM on a wave with length equal to the ship length and with specified steepness s_W.

In fact, except for cases where limitations are introduced by the ship depth and the full draught, in general, the two mentioned flat waterplanes are placed above and below the actual calculation draught considering a draught variation equal to $L{\cdot}s_W/2$, where L is the ship length and s_W is the wave steepness factor. Such distance basically corresponds to the amplitude of a wave having length equal to the ship length and steepness equal to s_W. Therefore, the upper and lower calculation draughts can be considered to be placed approximately at the wave crest and wave through, respectively.

Eventually, the approximate variation of metacentric height in waves, δGM_1, depends on the steepness factor s_W and, for standard environmental conditions (corresponding to unrestricted service), it is $s_W = 0.0167$.

Vulnerability at level 1 is checked by comparing the ratio $\delta GM_1/GM$ with a threshold value R_{PR}. Specifically, a loading condition is considered not to be vulnerable to the parametric rolling failure mode, if

$$\frac{\delta GM_1}{GM} \leq R_{PR} \tag{1}$$

For a proper application of this condition, it shall be implicitly assumed that $GM > 0$.

For completeness, it is noted that a further check is also present in the PR-L1 criterion, to guarantee that the vessel is not characterised by a tumblehome shape. In fact, the simplified procedure in PR-L1 is not intended for application to tumblehome vessels. For such special shapes, the analysis should be based on the other levels of assessment.

The threshold R_{PR} depends on the midship section coefficient at fully loaded departure condition and on the ratio $100A_k/LB$, where A_k is the area of the bilge keels, L is the ship length and B is the ship breadth. Larger values of $100A_k/LB$ lead to larger values of threshold R_{PR}.

In the PR-L2-C1 criterion, a loading condition is considered not vulnerable when the criterion $C1$ does not exceed a threshold $R_{PR1} = 0.06$. The criterion $C1$ is calculated as a weighted average of what could be referred to as "vulnerability indices", C_i, for a set of N wave cases, as follows:

$$C1 = \sum_{i=1}^{N} W_i C_i \tag{2}$$

Each "wave case" is associated with a weighting factor W_i and corresponds to a different regular wave with given length λ_i and height H_i. The corresponding index C_i can be either 0 or 1. Specifically, $C_i = 1$ when 2:1 parametric roll conditions in terms of parametric excitation magnitude and frequency can be fulfilled for the considered wave, and $C_i = 0$ otherwise.

For the inception of 2:1 parametric rolling, it is necessary that the magnitude of parametric excitation is sufficiently large, and the ship can achieve a speed leading to a 2:1 ratio between encounter frequency and roll natural frequency (corrected for variation of mean metacentric height). When any of the two conditions is not fulfilled, then basically the "wave case" is flagged as non-dangerous ($C_i = 0$).

For checking the condition related to the magnitude of parametric

excitation, stability calculations in waves are carried out. For each wave case corresponding to wave length λ_i and wave height H_i, the variation of GM is determined as $\delta GM(H_i,\lambda_i)$, while the average GM is determined as $GM(H_i,\ \lambda_i)$. The condition for the inception of 2:1 resonance is considered not to be fulfilled (hence $C_i = 0$) when, for a positive average GM, the parametric excitation is sufficiently small, i.e.:

$$GM(H_i,\lambda_i) > 0 \quad \text{and} \quad \frac{\delta GM(H_i,\lambda_i)}{GM(H_i,\lambda_i)} < R_{PR} \tag{3}$$

From (3) it can be seen that the threshold value R_{PR} plays a fundamental role both in PR-L1 and also in PR-L2-C1 assessment.

Regarding the frequency condition, this is checked in terms of comparison between the ship service speed, V_S, and the slowest speed leading to a 2:1 frequency ratio for the considered wave case, $V_{PR,i}$. The wave case is flagged with $C_i = 0$ if $V_{PR,i}$ exceeds V_S, i.e.

$$\begin{cases} V_{PR,i} > V_S \\ V_{PR,i} = \left| \frac{2\lambda_i}{T_r} \sqrt{\frac{GM(H_i,\lambda_i)}{GM}} - \sqrt{g\frac{\lambda_i}{2\pi}} \right| \text{ when } GM(H_i,\lambda_i) > 0 \end{cases} \tag{4}$$

where T_r is the ship natural roll period.

It is noted that both (3) and (4) apply when $GM(H_i,\lambda_i) > 0$. Wave cases such that the average metacentric height in the considered wave is non-positive, i.e. $GM(H_i,\ \lambda_i) \le 0$, are conventionally flagged as "dangerous" ($C_i = 1$).

For standard environmental conditions, wave cases (W_i,λ_i,H_i) for parametric rolling evaluation are 16 in total, and are specified in Table 2.5.3.2.3 of MSC.1/Circ.1627 (IMO, 2020).

Once MetOcean data are specified for the considered operational area, operational limitations can be embedded in parametric rolling vulnerability assessment by proper modification of wave-related calculation parameters in the vulnerability criteria. With reference to PR-L1 and PR-L2-C1 criteria, the implementation of alternative environmental data leads to a modification of the calculation wave cases in the PR-L2-C1 assessment and a corresponding modification of the wave steepness parameter s_w in the PR-L1 assessment.

The procedure for the definition of the wave cases in the PR-L2-C1 criterion and of the wave steepness in the PR-L1 criterion is described in the Explanatory Notes (IMO, 2019; 2021b). The procedure is based on the processing of the wave scatter table of significant wave height H_s and spectral period (typically, but not necessarily, the zero-crossing period T_z) for the considered area.

From the wave scatter table, a total of N wave cases are defined for the PR-L2-C1 assessment, where N corresponds to the number of cells of wave periods in the scatter table having non-zero marginal probability. Each "wave case" is characterised by a corresponding weighting factor W_i, wave length λ_i and wave height H_i, exactly as the standard wave cases in MSC.1/Circ.1627 (IMO, 2020).

The weighting factor W_i corresponds to the marginal probability of the corresponding cell of spectral period, as determined from the wave scatter table.

For the definition of the wave length λ_i of each wave case, a reference period $T_{ref,i}$ is firstly determined for each cell of wave spectral period. Specifically, $T_{ref,i}$ is defined as the mean spectral period, T_{01}. The determination of T_{01}, if not directly available, depends on the assumed spectral shape. In absence of alternative specific information, the framework in MSC.1/Circ.1627 (IMO, 2020) assumes a Bretschneider spectral shape.

The wave length λ_i is then calculated from $T_{ref,i}$ as:

$$\lambda_i = \frac{g \cdot T_{ref,i}^2}{2 \cdot \pi} \tag{5}$$

For the definition of the wave height H_i, first, the conditional average significant wave height for each spectral period, $E\{H_s|T_i\}$, is determined from the data in the wave scatter table. Then, the corresponding wave height H_i is defined as

$$\begin{cases} H_i = k_{PR} \cdot E\{H_s|T_i\} \\ \text{with } k_{PR} = 0.7 \end{cases} \tag{6}$$

The wave steepness parameter s_W for the PR-L1 vulnerability assessment is eventually defined as the maximum wave steepness among the wave cases defined for the PR-L2-C1 assessment, for reasons of conservativeness.

It should now be evident that differences in the reference wave scatter tables that may come from using different sources of data, lead to differences in the wave cases for the PR-L2-C1 assessment and in the wave steepness factor for the PR-L1 assessment. This eventually reflects in different outcomes regarding the identification of safe zones of loading conditions.

Therefore, the scope of this study is to provide a quantification of the level of variability that different sources of MetOcean data may induce in the stability assessment results.

3. Application

This section provides results for the main example application, which refers to a hull form representative of a RoPax ship. Following the same line of investigation as used in this section, additional results for the CEHIPAR2792 (Bulian et al., 2009, 2010) are reported in the Appendix.

3.1. Sample ship

The sample ship used in the application reported in this section is representative of a RoPax ship of about 160 m in length, shortly identified hereinafter as RP160. The main characteristics of the ship are reported in Table 1.

The ship is characterised by the presence of a ducktail and it is not fitted with bilge keels. Therefore, as a basis, the bilge keels area A_k is to be taken equal to 0 m^2 in the application of the vulnerability criteria. However, in order to provide an assessment of the effect of the bilge keels, an additional configuration has also been considered, with bilge keels characteristics as reported Table 2.

With reference to the application of vulnerability criteria from MSC.1/Circ.1627 (IMO, 2020), it is noted that, as an approximation, the length between perpendiculars in Table 1 is considered as reference ship length L. Furthermore, the draught corresponding to the fully loaded departure condition, d_{full}, has been assumed equal to the design draught T in Table 1.

A fundamental parameter for the application of PR-L1 and PR-L2-C1 vulnerability criteria is the R_{PR} coefficient (see §2.5.2.1 in MSC.1/Circ.1627 (IMO, 2020)), which essentially plays the role of the threshold value for the dimensionless variation of metacentric height (see eq. (1) and eq. (3)). The coefficient R_{PR} is strongly dependent on the bilge keels area ratio, with R_{PR} increasing as the bilge keels area ratio increases. The values of R_{PR} for the considered vessel, with and without bilge keels, are reported in Table 3.

According to Table 3, for the condition without bilge keels, R_{PR} takes the minimum regulatory value, i.e. 0.17. In the considered configuration with bilge keels, R_{PR} attains a value of 0.4753, which corresponds to about 2.8 times the value without bilge keels. This essentially means that, for given variation of metacentric height in waves, the minimum metacentric height to comply with the parametric excitation threshold requirement in case of the ship without bilge keels is almost three times

Table 1
RP160. Main characteristics.

Length between perpendiculars, L_{BP}	159.7 m
Breadth, B	24.8 m
Design draught, T	6.4 m
Service speed, V_S	27 knots

Table 2
RP160. Bilge keels characteristics.

Bilge keels length, l_{BK}	52.7 m
Bilge keels width, b_{BK}	0.4 m
Area of bilge keels, A_k	42.16 m^2
Length ratio, $l_{BK}/\ L_{BP}$	0.330
Width ratio, $b_{BK}/\ B$	0.0161
Area ratio, $A_k/\ (L_{BP}B)$	0.0106

Table 3
RP160. Values of coefficient R_{PR} with and without bilge keels, and corresponding ratio.

R_{PR} with bilge keels	0.4753
R_{PR} without bilge keels	0.1700
Ratio	2.796

smaller than the corresponding value for the ship equipped with the assumed bilge keels. As it will be clearly evident from the presentation of application results in section 3.3, the effect of bilge keels is significant.

3.2. Environmental data and derived calculation parameters

The Mediterranean Sea has been considered as operational area. Corresponding MetOcean data have been gathered from five different sources. Depending on the source, data have been gathered directly in the form of wave scatter tables, or as raw data from which wave scatter tables have been derived. In comparison with the previous initial work by Bulian and Orlandi (2021), two data sources used herein are in common, one data source has been updated, and two new data sources have been added.

In the following, first, a series of information are reported that are relevant to all considered data sources. Then, each data source is separately described.

3.2.1. Common considerations

A series of aspects are common to the analysis of all considered data, and are reported in the following.

According to MSC.1/Circ.1627 (IMO, 2020), operational limitations can be implemented considering environmental conditions relevant for a specific operational area or route and, if appropriate, specific season. Herein, data corresponding to all-year/all-directions have been used for all data sources, and this provides a distribution of environmental conditions that is considered to be representative of operation in the Mediterranean Sea for the whole year.

The procedure for the definition of the calculation parameters for PR-L1 and PR-L2-C1 assessment is based on the availability of a relevant wave scatter table (see IMO (2019; 2021b) and the description in section 2 herein). Depending on the data source, environmental conditions have been either directly collected in the form of wave scatter tables (for three data sources), or wave scatter tables have been created starting from samples of spectral period and significant wave height at different locations (for two data sources).

Wave scatter tables from all data sources have eventually been rounded to a precision of 10^{-4} for the probability associated to each discretization cell for the combination wave period-significant wave height.

In all cases, a Bretschneider spectral shape has been assumed, which is the standard spectral shape used in MSC.1/Circ.1627 (IMO, 2020). The assumption regarding the spectral shape may have an influence on the determination of the calculation parameters for PR-L1 and PR-L2-C1 assessment, depending on the provided data. This is indeed the case when the source data are provided in terms of a spectral period that is different from the mean period T_{01}, i.e. the period that is used for the definition of the reference wave length for wave cases in PR-L2-C1 assessment (see eq. (5)). According to the assumption of Bretschneider spectral shape, the following transformations hold among different periods:

$$\begin{cases} T_{01} = \dfrac{\pi^{1/4}}{\Gamma(3/4)} \cdot T_z \approx 1.0864348 \cdot T_z \\ T_{01} = \dfrac{(4/5)^{1/4}}{\Gamma(3/4)} \cdot T_p \approx 0.7717714 \cdot T_p \end{cases} \tag{7}$$

where $\Gamma(.)$ is the gamma function, T_p is the spectral peak period and T_z is the zero-crossing period.

The obtained wave cases for PR-L2-C1 assessment will be reported, for each data source, in specific corresponding tables. Each table will provide the wave case number, the wave length λ_i, the wave height $H_{PR,i}$ and the wave steepness $s_{W,PR,i} = H_{PR,i}/\lambda_i$. For reasons related to rounding, the tables will report integer counting factors K_i, and corresponding weighting factors W_i shall be determined from the factors K_i through normalization, i.e.

$$W_i = \frac{K_i}{\Sigma_j K_j} \tag{8}$$

In addition, each table will also report the maximum wave steepness among all PR-L2-C1 wave cases, which corresponds to the steepness factor s_W to be used for PR-L1 assessment (see section 2).

3.2.2. Dataset GWS

The first source of data is Global Wave Statistics Online (BMT, 2021), and, hereinafter, it is shortly referred to as "GWS".

Data from this dataset come from the processing of voluntary visual observations in the period 1854–1984 (BMT, 2021). Visual observations have been processed through the NMIMET data processing procedure (BMT, 2021), which makes use of observed wind speed and wave height, combined with parametric models for relevant marginal and/or joint distributions of wind speed, significant wave height and characteristic wave period. Observations of wave period were not used as they were found to be unreliable (BMT, 2021). Eventually, the application of the NMIMET data processing procedure to visual observations allowed to arrive at the definition of marginal and/or joint distributions of wind speed, wave height and characteristic zero-crossing period, for a set of geographical areas distributed worldwide.

Among the three considered dataset, this dataset can be regarded as the closest one to the background of the standard environmental conditions in MSC.1/Circ.1627 (IMO, 2020), which come from IACS Rec. 34 (IACS, 2001).

With reference to sea state, GWS data are provided in the form of wave scatter tables based on significant wave height and zero-crossing period.

In order to define a single wave scatter table that can be considered representative of the Mediterranean Sea, data for west (area 26) and east (area 27) Mediterranean Sea have been used. The two considered geographical areas are shown in the map in Fig. 1.

Wave scatter tables for area 26 and area 27 have been collected, and have then been averaged to obtain a single wave scatter table representative of the Mediterranean Sea. Since GWS wave scatter tables are provided in terms of zero-crossing period, T_z, a conversion to mean spectral period T_{01} has been carried out, following the assumption of Bretschneider spectral shape, according to eq. (7). Wave cases for PR-L2-C1 assessment, and the corresponding wave steepness factor for PR-L1 assessment, have then be derived from the averaged wave scatter table, in accordance with the procedure described in section 2.

In the analysis, some issues have been encountered in the processing of the wave scatter table obtained by averaging data from area 26 and area 27. Specifically, the cell resolution of the wave scatter table in terms of significant wave height is 1 m, and the resolution in terms of zero crossing period is 1 s. However, the cell of shortest zero-crossing periods covers a wider range, from 0 s to 4 s (BMT, 2021). This resolution is

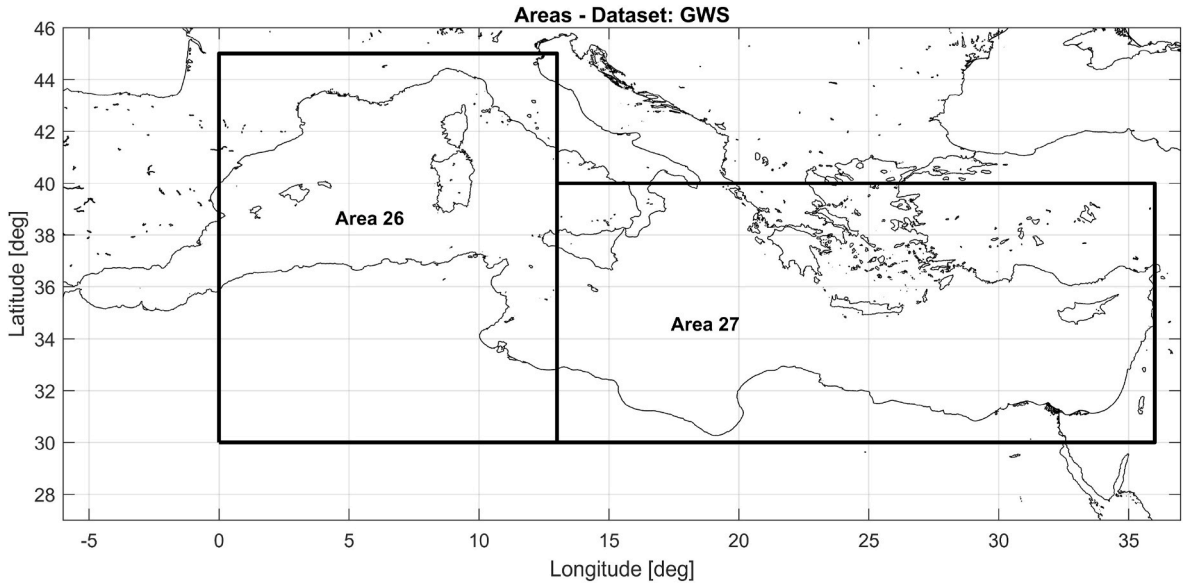

Fig. 1. Geographical areas considered in the GWS dataset.

coarse when it comes to the analysis of the region of small zero-crossing periods (hence short waves), and using the centre-cell for the range of T_z from 0 s to 4 s, i.e. $T_z = 2\ s$, leads to what appear to be too steep waves. To mitigate this issue, it was decided to associate a period $T_z = 3.5\ s$ to the lowermost cell, corresponding to the smallest zero-crossing periods with positive marginal probability in MSC.1/Circ.1627 (IMO, 2020) and IACS Rec. 34 (IACS, 2001). It is noted that the presence of too steep waves in the region of short periods has a direct consequence in the application framework, because, for the case of Mediterranean Sea, it leads to large values for the steepness factor for the PR-L1 assessment.

Results for the GWS dataset are reported in Table 4. It can be seen that the maximum wave steepness is associated with the wave case with the shortest wave length. This point will be subsequently discussed, as it is a critical point, which is common to all the considered datasets.

It is noted that there is a minor difference in the wave lengths reported in Table 4 and those reported by Bulian and Orlandi (2021) for the same dataset. This is due to the different rounding of the transformation factor between T_z and T_{01}. In particular, herein, more significant digits have been retained. However, the difference is minimal and practically negligible.

3.2.3. *Dataset Medatlas*

The second dataset considered in this study comes from the "Wind and Wave Atlas of the Mediterranean Sea" (Athanassoulis et al., 2004a), commonly known as "Medatlas", which is the short naming used hereinafter.

The Medatlas is a wind and wave atlas of the Mediterranean Sea, that has been produced using, as a basis, a 10-year (1992–2002) dataset of numerical MetOcean data coming from ECMWF atmospheric and wave models (Athanassoulis et al., 2004a,b; Cavaleri, 2005). Specifically, wave data were generated at EMCWF by the use of the WAM wave model (The WAMDI Group, 1988; Komen et al., 1994).

The reference dataset for the development of Medatlas comprised data from 935 locations and no use was made of visual estimates (Athanassoulis et al., 2004b). To increase the accuracy of the numerical dataset from the ECMWF model, a calibration procedure has been implemented exploiting a combined use of buoy and satellite measurements (Athanassoulis et al., 2004b; Cavaleri, 2005). The calibration procedure revealed to be particularly important for regions with complicated geometry and/or orography in the nearby land (Athanassoulis et al., 2004b).

The Medatlas provides MetOcean statistics for wind and waves on the whole Mediterranean, with a database of 239 locations (Athanassoulis et al., 2004a). Most of the points are provided on a lat/lon grid of $1^\circ \times 1^\circ$, with increased resolution in the Gulf on Lion, in the Ligurian, Northern Thyrrenian, Adriatic, Aegean and Cretan seas. A map reporting the 239 Medatlas locations is shown in Fig. 2.

For the purpose of this study, wave scatter tables have been collected for the 239 locations available from Medatlas. The 239 wave scatter tables have been subsequently averaged, to obtain a single wave scatter table representative of the whole Mediterranean Sea.

Since Medatlas wave scatter tables are provided in terms of peak spectral period, T_p, a conversion to mean spectral period T_{01} has been carried out, following the assumption of Bretschneider spectral shape, according to eq. (7). Wave cases for PR-L2-C1 assessment, and the corresponding wave steepness factor for PR-L1 assessment, have then be derived from the averaged wave scatter table, in accordance with the procedure described in section 2.

It is worth noting that the Medatlas wave scatter tables have a quite fine resolution in terms of periods and significant wave height in the region of short/low waves. This resolution is based on the frequency grid of the ECMWF-WAM model (Athanassoulis et al., 2004b) and it well adapts to the wave characteristics in the Mediterranean Sea.

Results from the Medatals dataset are reported in Table 5. It can be seen that, also for this dataset, the maximum wave steepness is associated with the wave case with the shortest wave length. The mentioned non-uniform resolution of the Medatlas wave scatter tables helps in partially controlling the calculated steepness of wave cases with short wave lengths. Nevertheless, still there seems to be a tendency to have

Table 4
Mediterranean Sea. Dataset: GWS. Wave cases for PR-L2-C1 assessment, and wave steepness factor for PR-L1 assessment (in bold and underlined).

Wave case number	K_i [-]	Wave length λ_i [m]	Wave height $H_{PR,i}$ [m]	Wave steepness $s_{W,PR,i}$ [-]
1	751	22.575	0.559	**<u>0.0248</u>**
2	2738	37.318	0.847	0.0227
3	3425	55.747	1.149	0.0206
4	2057	77.862	1.450	0.0186
5	765	103.662	1.745	0.0168
6	209	133.148	2.031	0.0153
7	46	166.320	2.252	0.0135
8	8	203.177	2.188	0.0108
Sum:	9999			

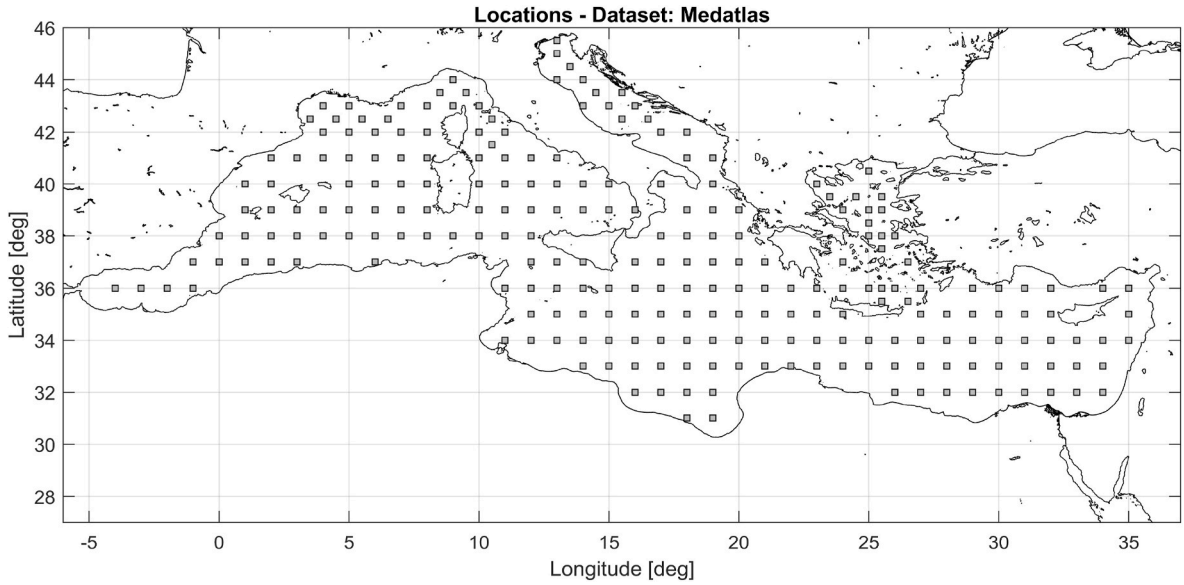

Fig. 2. Locations considered in the Medatlas dataset.

Table 5
Mediterranean Sea. Dataset: Medatlas. Wave cases for PR-L2-C1 assessment, and wave steepness factor for PR-L1 assessment (in bold and underlined).

Wave case number	K_i [-]	Wave length λ_i [m]	Wave height $H_{PR,i}$ [m]	Wave steepness $s_{W,PR,i}$ [-]
1	57	4.729	0.155	**0.0328**
2	181	7.554	0.198	0.0262
3	653	11.069	0.271	0.0245
4	1491	16.210	0.385	0.0238
5	1020	21.426	0.491	0.0229
6	1072	25.926	0.574	0.0221
7	1118	31.338	0.671	0.0214
8	1111	37.913	0.782	0.0206
9	1020	45.894	0.906	0.0197
10	860	55.568	1.058	0.0190
11	596	67.190	1.232	0.0183
12	408	81.213	1.437	0.0177
13	242	98.373	1.643	0.0167
14	105	119.168	1.813	0.0152
15	38	144.147	1.690	0.0117
16	10	174.418	0.945	0.0054
17	7	233.776	0.388	0.0017
18	5	340.505	0.088	0.0003
Sum:	9994			

somehow too large steepness values in case of short waves. It is also worth noting that the weighting factor for the wave case number 4 represents a sort of spike when compared to the wave cases number 3 and 5. This is likely linked with the non-uniform discretization of wave periods in the original Medatlas wave scatter tables, where the interval of wave periods associated with wave case number 4 is wider than those associated with the adjacent wave cases number 3 and number 5.

3.2.4. Dataset LaMMA

The third source of data is an in-house MetOcean dataset from Consorzio LaMMA, and it is therefore shortly referred to as "LaMMA".

At Consorzio LaMMA, different wind-wave operational forecasting systems have been implemented since 2006 (e.g. Orlandi et al., 2008, 2011; Pasi et al., 2011) and applied also to several navigation-related topics (Orlandi and Bruzzone, 2011; Ludeno et al., 2014; Orlandi et al., 2015, 2018, 2021). Most of the data produced by the operational forecasting activity at Consorzio LaMMA have been archived and are frequently utilized for several kinds of analyses. For this activity, the last decade of the longest of these operational datasets has been utilized. The dataset covers the period from 2010 to 2019 and has been generated by the third generation spectral wave forecasting NOAA model WAVEWATCH III® (WW3, 2021), forced by wind from limited area runs of the WRF mesoscale atmospheric model (WRF, 2021) with initial and boundary conditions from the NCEP GFS global model (GFS, 2021). The configuration of WRF and WW3 models covers the whole Mediterranean basin, with a constant resolution of about 12 km. WAVEWATCH III® runs have been initialized in hot start mode, through restart files from the antecedent run. The operational configuration comprised two runs each day (with initialization times at 00 UTC and 12 UTC), each one covering the next five days. The set of data used in this work has an hourly time step and has been generated by extracting only the first 24 h of forecast data from each daily operational run. This allowed to uniformly cover the whole decade with data having the highest available accuracy (i.e. the nearest to the initialization time) from each forecast run. Only few days in the considered decade resulted with no data, due to very rare malfunction of the forecasting system.

Generally, a decadal dataset generated from operational forecasts may not be to the same level as, for instance, a dataset obtained by a multi-decadal hindcast reanalysis. However, the background data for the LaMMA dataset have been uniformly generated by a constant model setup, and the model showed good operational performance as indicated by comparisons with observed data (Orlandi et al., 2011). In particular, comparisons with observations indicated a good time phasing for most of the relevant meteo-marine dynamics and events, with a tendency to slightly underestimate some of the wave height peaks and to slightly underestimate the average wave period (Orlandi et al., 2011).

In the previous work by Bulian and Orlandi (2021), 61 locations on a uniform $2^\circ \times 2^\circ$ lat/lon grid were used to gather MetOcean data. In the present work the background dataset has been increased, and data have been gathered from a finer uniform $1^\circ \times 1^\circ$ lat/lon grid, corresponding to 247 locations. A map reporting the 247 LaMMA locations is shown in Fig. 3.

The distribution of locations for the LaMMA dataset (Fig. 3) is, to a very large extent, similar to that for the Medatlas dataset (Fig. 2). However, while the locations in the LaMMA dataset are associated to a fully uniform $1^\circ \times 1^\circ$ lat/lon grid, the Medatlas dataset shows some refined gridding in some specific areas (see section 3.2.3 and Fig. 2).

The characteristic period for this dataset is the mean spectral wave period T_{01}, that can directly be used for the determination of wave cases for the PR-L2-C1 assessment.

The reference wave scatter table for the application of the procedure

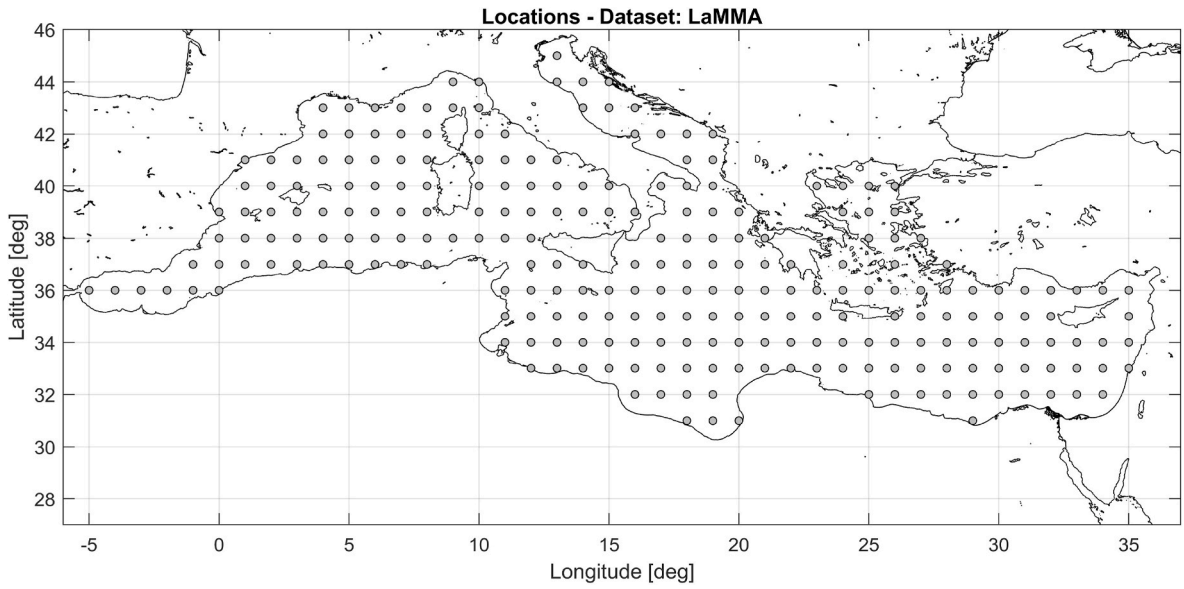

Fig. 3. Locations considered in the LaMMA dataset.

described in section 2, was developed from the available data by using a fine discretization both for the mean spectral wave period and for the significant wave height, using cells having width of 0.5 s and 0.25 m, respectively. Such discretization appears to be appropriate in most of the regions of period and significant wave height. However, the resolution of significant wave height in the region of very short waves is still too coarse, and the data discretization leads, also for this dataset, to high conditional mean steepness in the region of very short periods.

Results for the LaMMA dataset are reported in Table 6. It can be seen that, also for this dataset, the maximum wave steepness is associated with the wave case with the shortest wave length.

It is worth noting that results obtained in Table 6 are very close to those previously obtained by Bulian and Orlandi (2021) using the same background MetOcean data, but considering a coarser grid ($2^\circ \times 2^\circ$ vs $1^\circ \times 1^\circ$), corresponding to a reduced number of locations (61 vs 247).

3.2.5. *Dataset KNMI*

The fourth dataset considered in this study comes from the "KNMI/ERA-40 Wave Atlas" (Sterl and Caires, 2006), and it is shortly referred herein as "KNMI".

The KNMI wave atlas provides worldwide statistics for sea state parameters and wind speed. Numerous information are provided related to wind and wave climate and climate variability. For the specific case of the present study, the interest is on the availability of bivariate histograms, i.e. scatter tables, for significant wave height and zero-crossing period. These data are provided by the KNMI Wave Atlas on geographical areas with $9^\circ \times 9^\circ$ lat/lon extension.

The background data for the KNMI wave atlas come from the ERA-40 reanalysis developed by the ECMWF (Uppala et al., 2005), spanning the period from September 1957 to August 2002. However, only the period 1971–2000 has been actually used in the preparation of the KNMI wave atlas, in order to have a 30-year dataset in accordance with the recommendations from the World Meteorological Organization (Sterl and Caires, 2006).

In connection with the preparation of the KNMI wave atlas, some deficiencies were identified in the ERA-40 dataset regarding the significant wave height (Caires and Sterl, 2005; Sterl and Caires, 2006). According to Caires and Sterl (2005) and Sterl and Caires (2006), the ERA-40 dataset suffers from two main relevant limitations, namely inhomogeneity in time and underestimation of high significant wave heights. To try overcoming the identified limitations, a correction methodology was developed (Caires and Sterl, 2005) and it was used to improve the ERA-40 data, leading to what is referred to as the "corrected ERA-40" (C-ERA-40) dataset (Caires and Sterl, 2005; Sterl and Caires, 2006). The comparison of C-ERA-40 data with buoy and altimeter data showed clear improvements compared to the raw ERA-40 dataset (Caires and Sterl, 2005; Sterl and Caires, 2006).

Processed information are available in the KNMI wave atlas both using the ERA-40 and the C-ERA-40 databases. Considering the reported improvement obtained by the correction methodology (Caires and Sterl, 2005; Sterl and Caires, 2006), reference for this study was made to data based on the C-ERA-40 dataset.

It worth noting that the ERA-40 reanalysis (Uppala et al., 2005) is now considered to be superseded by the more recent ERA5 reanalysis (ECMWF, 2021). However, this is not reducing the value and the relevance of the KNMI wave atlas for the present study, considering also that it benefitted from the improved C-ERA-40 data (Caires and Sterl, 2005; Sterl and Caires, 2006). Furthermore, the KNMI wave atlas is based on more recent and advanced data compared to, e.g., the commonly used GWS dataset, which further supports the use of the KNMI dataset for the present study.

Table 6
Mediterranean Sea. Dataset: LaMMA. Wave cases for PR-L2-C1 assessment, and wave steepness factor for PR-L1 assessment (in bold and underlined).

Wave case number	K_i [-]	Wave length λ_i [m]	Wave height $H_{PR,i}$ [m]	Wave steepness $s_{W,PR,i}$ [-]
1	27	2.440	0.088	**0.0361**
2	254	4.782	0.108	0.0226
3	813	7.904	0.195	0.0247
4	1363	11.807	0.285	0.0241
5	1579	16.491	0.399	0.0242
6	1492	21.956	0.527	0.0240
7	1264	28.201	0.683	0.0242
8	1002	35.227	0.862	0.0245
9	748	43.034	1.065	0.0247
10	529	51.621	1.284	0.0249
11	359	60.989	1.537	0.0252
12	235	71.137	1.832	0.0258
13	146	82.066	2.149	0.0262
14	86	93.776	2.495	0.0266
15	49	106.267	2.884	0.0271
16	25	119.538	3.315	0.0277
17	8	133.590	4.200	0.0314
18	1	148.422	4.813	0.0324
Sum:	9980			

In order to define a single wave scatter table that can be considered representative of the Mediterranean Sea, a set of six geographical areas from the KNMI wave atlas have been considered, as shown in the map in Fig. 4. The figure reports also the minimum and maximum latitude and longitude for each area.

As anticipated, reference was made to KNMI wave scatter tables of significant wave height and zero crossing period, developed from the C-ERA-40 data. The wave scatter tables were averaged to obtain a single wave scatter table that was considered to be representative for the Mediterranean Sea. Since KNMI wave scatter tables are provided in terms of zero-crossing period, T_z, a conversion to mean spectral period T_{01} has been carried out, following the assumption of Bretschneider spectral shape, according to eq. (7). Wave cases for PR-L2-C1 assessment and corresponding wave steepness factor for PR-L1 assessment, have then be derived from the averaged wave scatter table, in accordance with the procedure described in section 2.

In the analysis, some issues have been encountered in the processing of the wave scatter table obtained by averaging those from the six considered areas. Similarly to the case of GWS data, the cell resolution of the wave scatter table in terms of significant wave height is 1 m, and the resolution in terms of zero crossing period is 1 s, but the cell of shortest zero-crossing periods covers a wider range, from 0 s to 3 s. This resolution, although better than in GWS tables, is still too coarse when processing data in the region of small zero-crossing periods (hence short waves). Using the centre-cell for the range of T_z from 0 s to 3 s, i.e. $T_z = 1.5\ s$, results in high steepness values driven by the discretization. In order to mitigate this issue, similarly to what was done in case of GWS data, a period $T_z = 2.5\ s$ has been associated to the lowermost cell. This leads to a constant stepping of T_z across different cells. Nevertheless, it is an arbitrary assumption, and, as it will be clear from the obtained data, it has an impact on the application in the framework of MSC.1/Circ.1627 (IMO, 2020).

Results for the KNMI dataset are reported in Table 7. It can be seen that, also for this dataset, the maximum wave steepness is associated with the wave case with the shortest wave length.

3.2.6. *Dataset CMEMS-MED*

The fifth considered dataset comes from the processing of a set of reanalysis hindcast data for the Mediterranean Sea, provided through the Copernicus Marine Service - CMES (CMEMS, 2021), and it is therefore referred to as CMEMS-MED.

Table 7
Mediterranean Sea. Dataset: KNMI. Wave cases for PR-L2-C1 assessment, and wave steepness factor for PR-L1 assessment (in bold and underlined).

Wave case number	K_i [-]	Wave length λ_i [m]	Wave height $H_{PR,i}$ [m]	Wave steepness $s_{W,PR,i}$ [-]
1	1164	11.518	0.371	**<u>0.0322</u>**
2	4314	22.575	0.576	0.0255
3	2948	37.318	0.870	0.0233
4	1185	55.747	1.215	0.0218
5	322	77.862	1.591	0.0204
6	58	103.662	1.883	0.0182
7	9	133.148	1.594	0.0120
8	1	166.320	0.350	0.0021
9	1	203.177	0.350	0.0017
Sum:	10002			

Specifically, data from the CMEMS product MEDSEA_MULTIYEAR_WAV_006_012 (Korres et al., 2019) were used. Details regarding the product are available in the respective accompanying documentation (Zacharioudaki et al., 2020; Korres et al., 2021), and a brief summary is reported in the following. The product provides reanalysis wave data starting from 1993. Data are provided on an hourly basis, on a fine grid of locations that covers the Mediterranean Sea and part of the east Atlantic Ocean (up to 18.125°W), with a lat/lon grid resolution of 1/24°x1/24°. Wave data are generated from a WAM Cycle 4.6.2 wave model (The WAMDI Group, 1988; Komen et al., 1994; Janssen, 2002). In order to properly simulate swells propagating from the North Atlantic and entering the Mediterranean Sea through Gibraltar, the forecasting system is based on the nesting of a coarse grid covering the Atlantic Ocean (lat/lon resolution 1/6°x1/6°) and the final 1/24°x1/24° fine grid. The wave model for the reanalysis is forced by interpolated wind speeds, at 10 m above sea level, coming from the ERA5 reanalysis (ECMWF, 2021). Further, wave data are subject to an assimilation process, inherent in WAM Cycle 4.6.2, where the wave spectrum is adjusted making use of observations from altimeters data, based on a procedure, initially developed by Lionello et al. (1992), and described by Zacharioudaki et al. (2020). Further information on the used upstream datasets regarding atmospheric forcing, sources for altimeter data, surface current forcing and sea-ice cover, as well as validation information, are available from Zacharioudaki et al. (2020).

Background data for the CMEMS-MED dataset have been gathered from the available grid of locations, considering only the locations

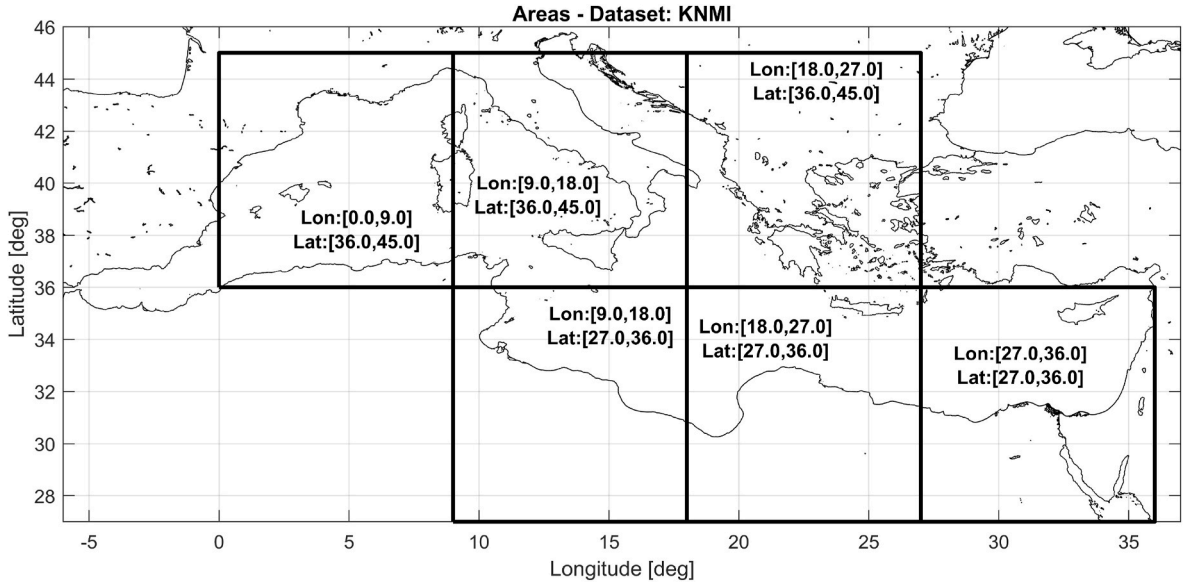

Fig. 4. Geographical areas considered in the KNMI dataset.

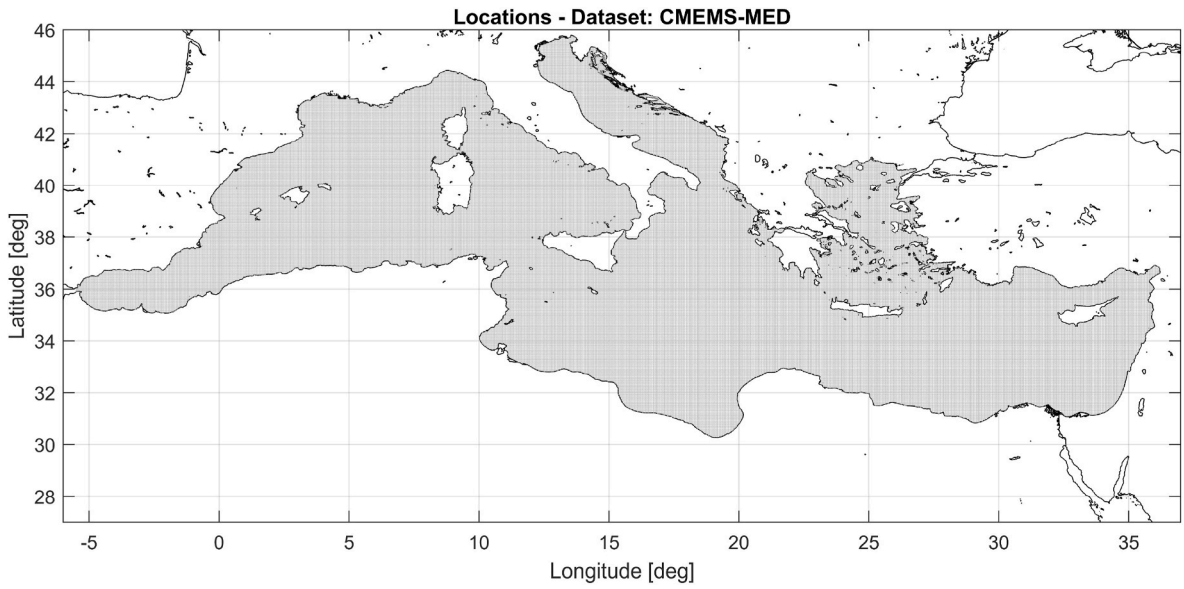

Fig. 5. Locations considered in the CMEMS-MED dataset.

covering the Mediterranean Sea, for a total of 144911 locations. The whole set of locations used for the present analysis is reported in Fig. 5. Considering the fine grid resolution, Fig. 5 is valuable in showing the considered area in the CMEMS-MED dataset, but single locations are hardly visible. Therefore, two representative zoom are shown in Fig. 6, to better appreciate the grid resolution.

For this study, the analysis was based on data covering the period 1993–2019, i.e. a total of 27 years, and the analysis used the significant wave height and the zero crossing period (variables Hm0 and Tm02 in the reanalysis dataset). For each location, hourly significant wave height and zero crossing period were collected for the whole 27-year timespan, leading to a total number of samples slightly above $3.4 \cdot 10^{10}$. This is a very large number of samples, but it should be borne in mind that the samples are generally characterised by statistical dependence for locations that are close each other in space, and/or samples that are close each other in time.

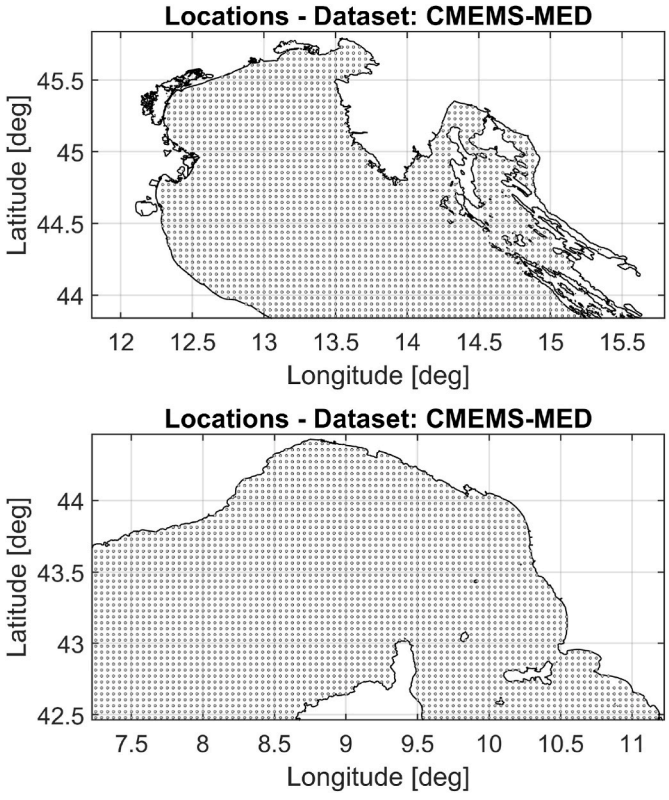

Fig. 6. Locations considered in the CMEMS-MED dataset. Zoom on two smaller representative areas.

All samples were used for defining a wave scatter table to which the procedure described in section 2 was applied. The resolution of the generated wave scatter table was 0.25 m for the significant wave height, and 0.5 s for the zero crossing period. This resolution is similar to that used for the LaMMA dataset, although for the LaMMA dataset the reference period is the mean spectral period T_{01} whereas the analysis of the CMEMS-MED dataset is based on the zero crossing period T_z. Therefore, the application of the procedure in section 2 required the conversion of the zero crossing period to the mean spectral period, and this was done in accordance with eq. (7).

Results for the CMEMS-MED dataset are reported in Table 8. It can be seen that, also for this dataset, the maximum wave steepness is associated with the wave case with the shortest wave length, and the wave steepness is extremely large. This is a consequence of the fact that the shortest considered wave length is indeed very short, namely about 1 m.

Table 8
Mediterranean Sea. Dataset: CMEMS-MED. Wave cases for PR-L2-C1 assessment, and wave steepness factor for PR-L1 assessment (in bold and underlined).

Wave case number	K_i [-]	Wave length λ_i [m]	Wave height $H_{PR,i}$ [m]	Wave steepness $s_{W,PR,i}$ [-]
1	2	1.037	0.088	**0.0849**
2	57	2.879	0.088	0.0306
3	327	5.644	0.134	0.0237
4	938	9.330	0.237	0.0254
5	1610	13.937	0.354	0.0254
6	1780	19.465	0.489	0.0251
7	1606	25.915	0.650	0.0251
8	1279	33.287	0.836	0.0251
9	929	41.580	1.043	0.0251
10	624	50.794	1.277	0.0251
11	392	60.930	1.529	0.0251
12	230	71.987	1.812	0.0252
13	125	83.966	2.146	0.0256
14	62	96.866	2.473	0.0255
15	27	110.688	2.797	0.0253
16	5	125.431	2.818	0.0225
Sum:	9993			

Therefore, the resolution of the wave scatter table in terms of significant wave height (0.25 m) is too coarse to properly resolve the appropriate value of conditional average significant wave height. In fact, it can be noticed that the wave steepness rapidly drops when the reference wave length increases.

3.2.7. Comments on the results

From the reported results in Tables 4–8, it can be seen that different sources of data lead to clearly different sets of wave cases for PR-L2-C1 assessment, and to significantly different values of wave steepness factor for PR-L1 vulnerability assessment.

To have a visual summary overview of the obtained differences, Fig. 7 shows the wave steepness as function of the wave length for PR-L2-C1 wave cases, as obtained from the different data sources. The wave case with maximum wave steepness, for each dataset, is indicated by a circle and the legend of the graph reports the corresponding value of wave steepness factor s_W for PR-L1 assessment. For the case of the CMEMS-MED dataset, the wave case #1, which is the one associated with the shortest wave length and the largest wave steepness, is out of the graph scale, and it is therefore indicate by a text box.

From the data in Tables 4–8 and from the graphical representation in Fig. 7 it can be seen that different data sources show qualitatively different behaviours. For GWS, Medatlas and KNMI datasets, the wave steepness decreases as the wave length increases. Instead, for the LaMMA dataset, the wave steepness tends to increase with the increase of the wave length. For the CMEMS-MED dataset the wave steepness is essentially constant in the core range, with a reduction tendency for the longest wave. In all cases, with the exception of the KNMI dataset, there is a sharp increase of the wave steepness in the short waves region, and, in particular, for the shortest available wave. This is a consequence of the reduced resolution of the wave scatter tables that does not allow to properly resolve the necessary information in the range of short wave lengths. The issue is particularly evident for the CMEMS-MED dataset, for which, according to the used discretization in the generation of the wave scatter table, the wave case with shortest wave is associated with a wave length just slightly above 1 m. As a result, for all sources, the maximum wave steepness, which is eventually to be used for PR-L1 assessment, is obtained for the wave case associated with the shortest wave length. This is valid also for the KNMI dataset. Furthermore, in all cases the maximum wave steepness is larger than the standard wave steepness for unrestricted service (i.e. $s_W = 0.0167$).

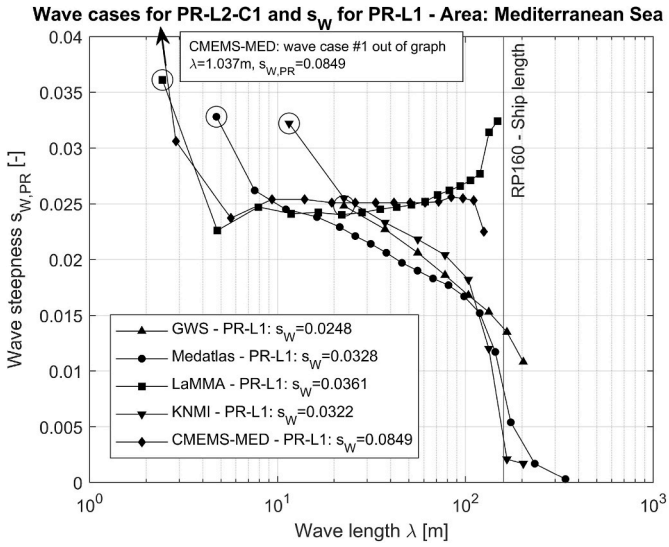

Fig. 7. Wave steepness as function of the wave length for PR-L2-C1 wave cases, as obtained from the different data sources. The wave case with maximum wave steepness, for each dataset, is indicated by a circle and the legend of the graph reports the corresponding value of wave steepness factor s_W for PR-L1 assessment.

Notwithstanding the observed critical issue, in compliance with the approach specified by the framework of SGISC, the obtained maximum steepness values have actually been used for PR-L1 vulnerability assessment (see results in the following section 3.3).

Comparing Tables 4–8, it can be clearly noticed that the wave cases obtained from the considered datasets are characterised by different wave lengths and associated weighting factors. This essentially reflects the different underlying distributions of wave periods in the original wave scatter tables. Fig. 8 shows a graphical comparison of weighting factors W_i as function of the wave length λ for PR-L2-C1 wave cases, as obtained from the different sources.

Looking at Fig. 8, it can be noticed that wave cases from GWS and Medatlas datasets tend to be shifted towards, and to give more weight to, longer waves compared to the other datasets.

In order to have a better understanding of the differences among the considered datasets, it is worth comparing also the mean wave length, λ_{mean}, and mean wave steepness, $s_{W,PR,mean}$, for each dataset. Such mean values have been calculated from the data in Tables 4–8, as

$$\begin{cases} \lambda_{mean} = \sum_i W_i \cdot \lambda_i = \left(\sum_i K_i \cdot \lambda_i \right) \Big/ \sum_i K_i \\ s_{W,PR,mean} = \sum_i W_i \cdot s_{W,PR,i} = \left(\sum_i K_i \cdot s_{W,PR,i} \right) \Big/ \sum_i K_i \end{cases} \tag{9}$$

Resulting mean values are reported in Table 9 and, graphically, in Fig. 9.

From the results in Table 9 and Fig. 9 it can be seen that LaMMA, KNMI and CMEMS-MED datasets are associated with mean values of wave length and steepness for PR-L2-C1 assessment that are close each other. The mean wave length in case of Medatlas dataset is larger than those from the three previously mentioned datasets, corresponding to about +27% with respect to the mean of the values for LaMMA, KNMI and CMEMS-MED. The mean wave steepness for the Medatlas dataset is, instead, smaller, corresponding to about −14% with respect to the mean of the value for LaMMA, KNMI and CMEMS-MED. The GWS dataset is characterised by the smallest average wave steepness, about −17% compared to the average value for LaMMA, KNMI and CMEMS-MED, with a value that is close to, and only −3% with respect to the average value for Medatlas. However, the average wave length for the GWS dataset is significantly larger than the average wave lengths associated with the other datasets, i.e. +99% (basically double) with respect to the average value for LaMMA, KNMI and CMEMS-MED, and about +57% with respect to the value for the Medatlas dataset.

Such differences in the average values of the length and steepness of wave cases for PR-L2-C1 assessment should be borne in mind when looking at the PR-L2-C1 calculation results in the following section 3.3.

With reference to results in Table 9 and Fig. 9, it is also worth mentioning that the GWS dataset is the only one in this study that is based on visual observations, while all the other datasets are based on data from numerical models with or without calibration/assimilation. Furthermore, it is also useful to note that the Medatlas dataset is the only one in this study that is based on the peak spectral period, while all the other datasets are based on reference periods (zero-crossing period or mean period) obtained from spectral moments, i.e. from integral quantities derived from the sea spectrum.

3.3. Safe zones

The determination of safe zones of loading conditions has been carried out for the sample ship (see section 3.1), considering zero trim. The assessment has been carried out both for the actual ship configuration, i.e. without bilge keels, as well as considering a configuration with bilge keels according to Table 2. PR-L1 and PR-L2-C1 vulnerability assessment criteria have been applied considering the calculation parameters (s_W for PR-L1, wave cases for PR-L2-C1), as obtained from the

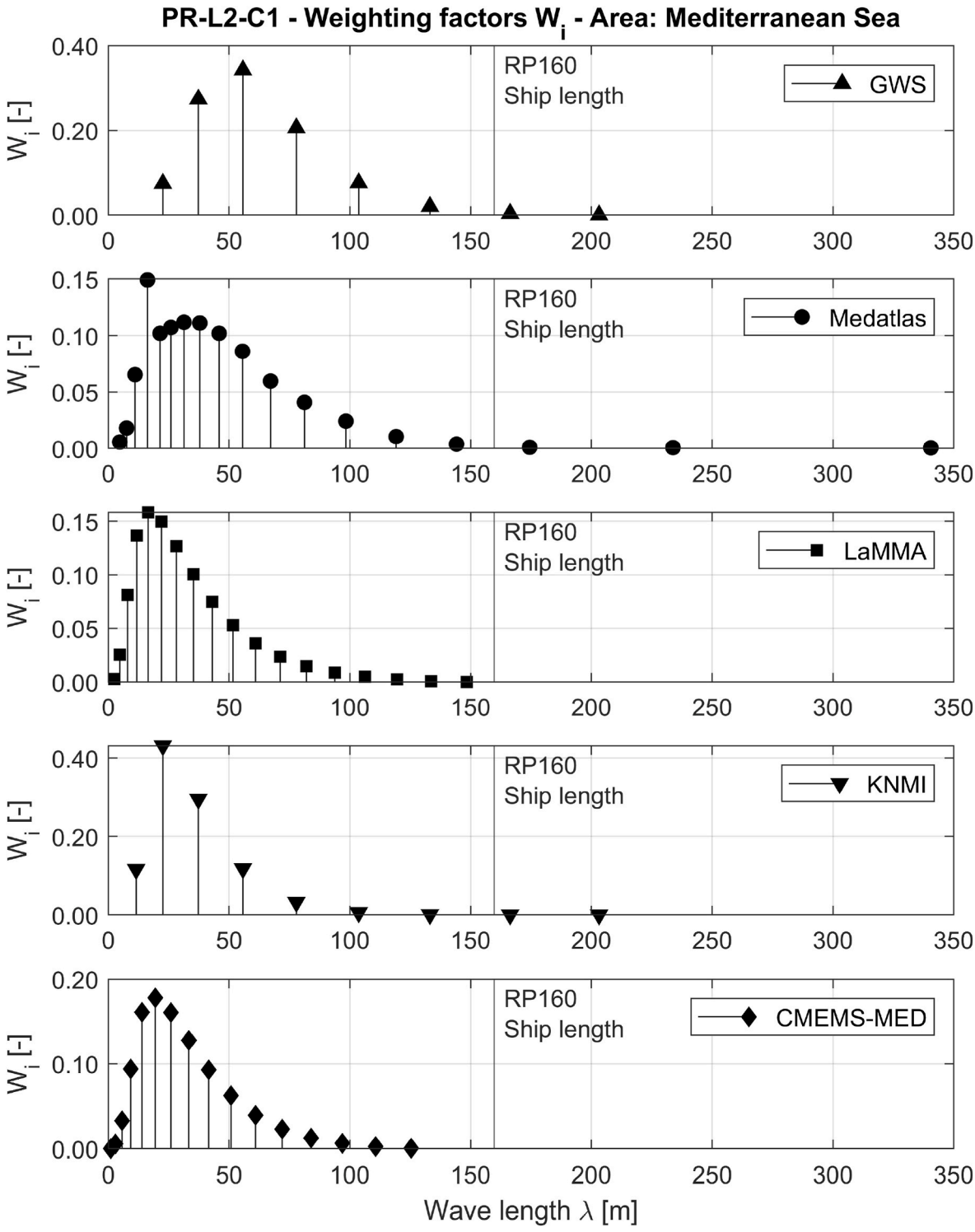

Fig. 8. Weighting factor as function of the wave length for PR-L2-C1 wave cases, as obtained from the different data sources.

Table 9
Mediterranean Sea. Mean wave length and wave steepness for wave cases for PR-L2-C1 assessment for each considered dataset.

Dataset	Mean wave length λ_{mean} [m]	Mean wave steepness $s_{W,PR,mean}$ [-]
GWS	58.669	0.0206
Medatlas	37.472	0.0213
LaMMA	28.167	0.0244
KNMI	31.946	0.0250
CMEMS-MED	28.312	0.0252

different sources (Table 4, Table 5, Table 6, Table 7 and Table 8).

In general, the application of second generation intact stability criteria is not guaranteed to lead to a classical curve of minimum *GM* /maximum *KG*, because it is generally not guaranteed that an increase of metacentric height always leads to a safer condition. Therefore, so-called "matrix calculations" shall be performed. This is clearly specified in MSC.1/Circ.1627 (IMO, 2020) as a general approach for all failure modes and, specifically for parametric rolling, in §2.5.1.4 therein.

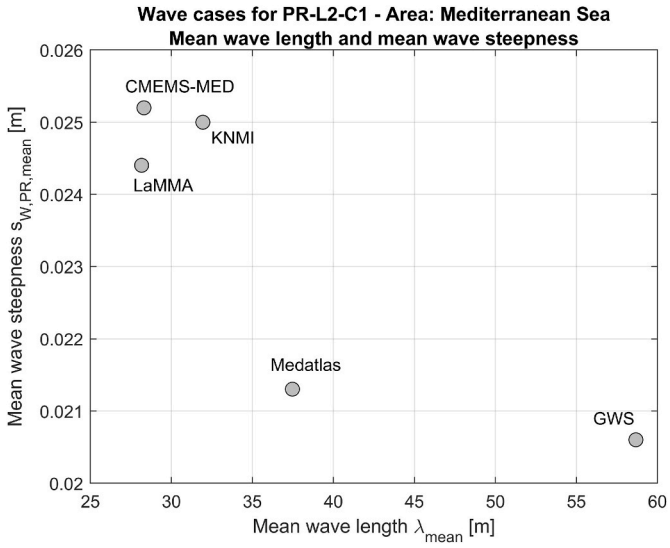

Fig. 9. Mediterranean Sea. Mean wave length and wave steepness for wave cases for PR-L2-C1 assessment for each considered dataset.

However, the structure of the PR-L1 criterion for parametric rolling is such that it actually leads to a curve of minimum *GM* /maximum *KG*. In fact, considering as given for granted that the analysis is carried out for conditions with positive calm water *GM*, condition (1) can be rewritten as

$$GM \geq \frac{\delta GM_1}{R_{PR}} \Rightarrow GM_{min} = \frac{\delta GM_1}{R_{PR}} \tag{10}$$

where the approximate fluctuation of the height of metacentre, δGM_1, depends on the steepness factor s_W, but not on the calm water *GM* itself (see §2.5.2.1 in MSC.1/Circ.1627 (IMO, 2020)).

In addition, for the ship under consideration, the application of the PR-L2-C1 criterion in the chosen range of draughts and metacentric heights led to the identification of a unique boundary between safe and unsafe regions of loading conditions.

These preliminary considerations allow to simplify the presentation of the results.

For the sake of reference and completeness, the assessment is carried out also using the standard environmental conditions for unrestricted service, as specified in MSC.1/Circ.1627 (IMO, 2020). For ease of reference, standard wave cases for PR-L2-C1 assessment and corresponding standard wave steepness factor for PR-L1 assessment (s_W = 0.0167) are reported in Table 10. The corresponding mean wave length, λ_{mean}, and mean wave steepness, $s_{W,PR,mean}$, determined according to eq. (9), are $\lambda_{mean} = 149.658\ m$ and $s_{W,PR,mean} = 0.0162$.

Table 10
Standard environmental conditions for unrestricted service, according to MSC.1/Circ.1627 (IMO, 2020). Wave cases for PR-L2-C1 assessment, and wave steepness factor for PR-L1 assessment (in bold and underlined).

Wave case number	W_i [-]	Wave length λ_i [m]	Wave height $H_{PR,i}$ [m]	Wave steepness $s_{W,PR,i}$ [-]
1	0.000013	22.574	0.350	0.0155
2	0.001654	37.316	0.495	0.0133
3	0.020912	55.743	0.857	0.0154
4	0.092799	77.857	1.295	0.0166
5	0.199218	103.655	1.732	**0.0167**
6	0.248788	133.139	2.205	0.0166
7	0.208699	166.309	2.697	0.0162
8	0.128984	203.164	3.176	0.0156
9	0.062446	243.705	3.625	0.0149
10	0.024790	287.931	4.040	0.0140
11	0.008367	335.843	4.421	0.0132
12	0.002473	387.440	4.769	0.0123
13	0.000658	442.723	5.097	0.0115
14	0.000158	501.691	5.370	0.0107
15	0.000034	564.345	5.621	0.0100
16	0.000007	630.684	5.950	0.0094
Sum:	1.000000			

3.3.1. PR-L1 assessment

Safe zones from PR-L1 assessment are identified by the limiting metacentric height GM_{min}, calculated according to eq. (10). Accordingly, GM_{min} depends on the ratio between the approximate fluctuation of the height of metacentre, δGM_1, and the threshold value R_{PR}. The threshold value R_{PR} depends on whether the ship is equipped with bilge keel or not (see Table 3). However, the fluctuation δGM_1 only depends on the ship geometry, loading condition and wave steepness factor s_W used in the calculations. Therefore, it is worth first reporting, in Fig. 10, the calculated values of δGM_1. PR-L1 calculations reported hereinafter have been carried out with a draught discretization of 0.05 m.

The curves of δGM_1 in Fig. 10 show a large variability depending on the source of data, and the ordering of the curves follows the ordering of the wave steepness factor s_W. It is also worth noting that δGM_1 calculated for unrestricted service is smaller than all the other cases, and this is a consequence of the fact that the steepness factor s_W for standard environmental conditions is the smallest among the considered cases.

Limiting metacentric heights GM_{min} can be determined directly from data reported in Fig. 10, using eq. (10) and the relevant threshold value R_{PR} (see Table 3). Fig. 11 shows the safe zones as obtained from the application of PR-L1 vulnerability assessment for the ship without and with bilge keels. Specifically, the curves reported in Fig. 11 represent the boundaries between safe and unsafe regions according to PR-L1 assessment.

From the results in Fig. 11, a series of considerations can be made. First, it can be seen that differences in the results stemming from the use of different sources of MetOcean data are very large. The differences are larger, in absolute sense, for the ship without bilge keels (Fig. 11-left) and are smaller, though large, in the ship configuration with bilge keels (Fig. 11-right). This is a direct consequence of the difference in the value of R_{PR} for the two configurations (see Table 3) and the relation between R_{PR} and the limiting metacentric height (see eq. (10)). However, in relative terms, the differences of limiting metacentric height among different sources are the same, again as a consequence of the relation (10). The ordering of limiting *GM* curves follows the ordering in the steepness parameter s_W obtained from the different sources, and this is a consequence of the fact that δGM_1 generally tends to increase with the

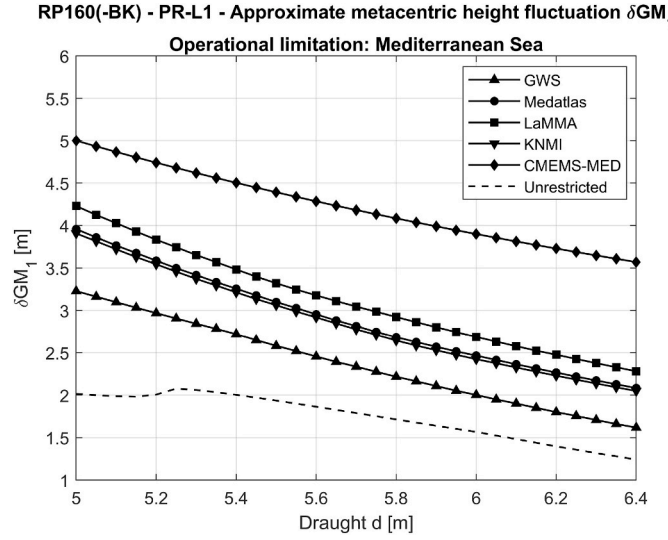

Fig. 10. RP160. Approximate metacentric height fluctuation, δGM_1.

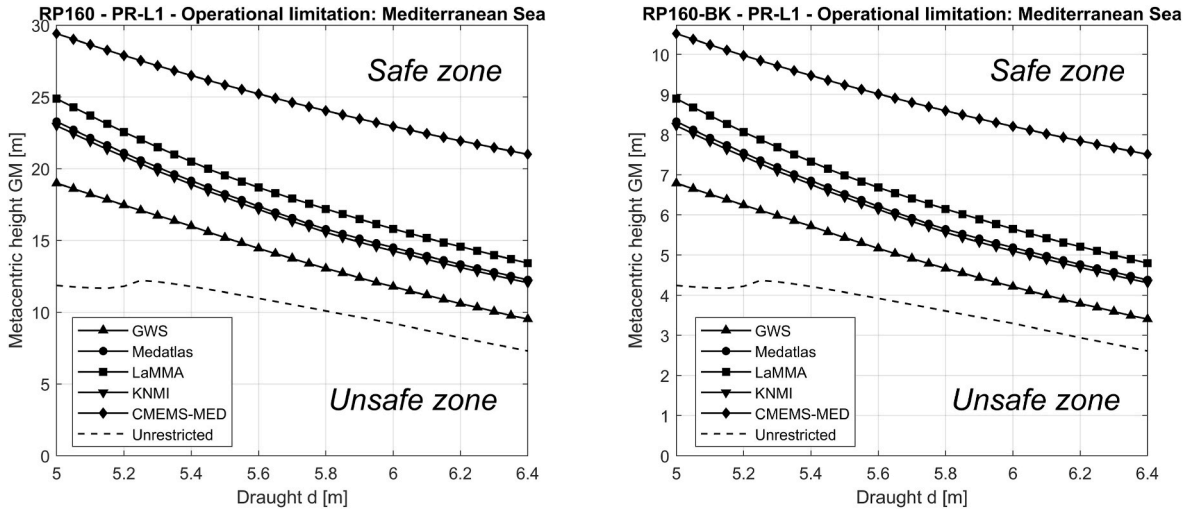

Fig. 11. RP160. Safe zones from PR-L1 vulnerability assessment for parametric rolling. Ship without bilge keels (left) and with bilge keels (right).

increase of s_W (see Fig. 10). It can also be noted that, in all cases, for the considered area, the limiting metacentric heights under operational limitations are larger than the limiting metacentric height obtained for unrestricted service.

At the same time, the PR-L1 assessment provides safe zones at values of *GM* that are unrealistically large for the considered ship. Such very high required *GM* are the result of the combination of multiple factors. First, stability variations from the simplified PR-L1 approach, i.e. the parameter δGM_1, generally tend to be conservative compared to direct calculations in waves. Then, the hull shape is characterised by flared forms, which tend to lead to stability variations in waves. Finally, for the condition without bilge keels, the threshold R_{PR} takes its minimum value, 0.17, and this leads to high values of the required *GM* given the variation of *GM*, according to eq. (10).

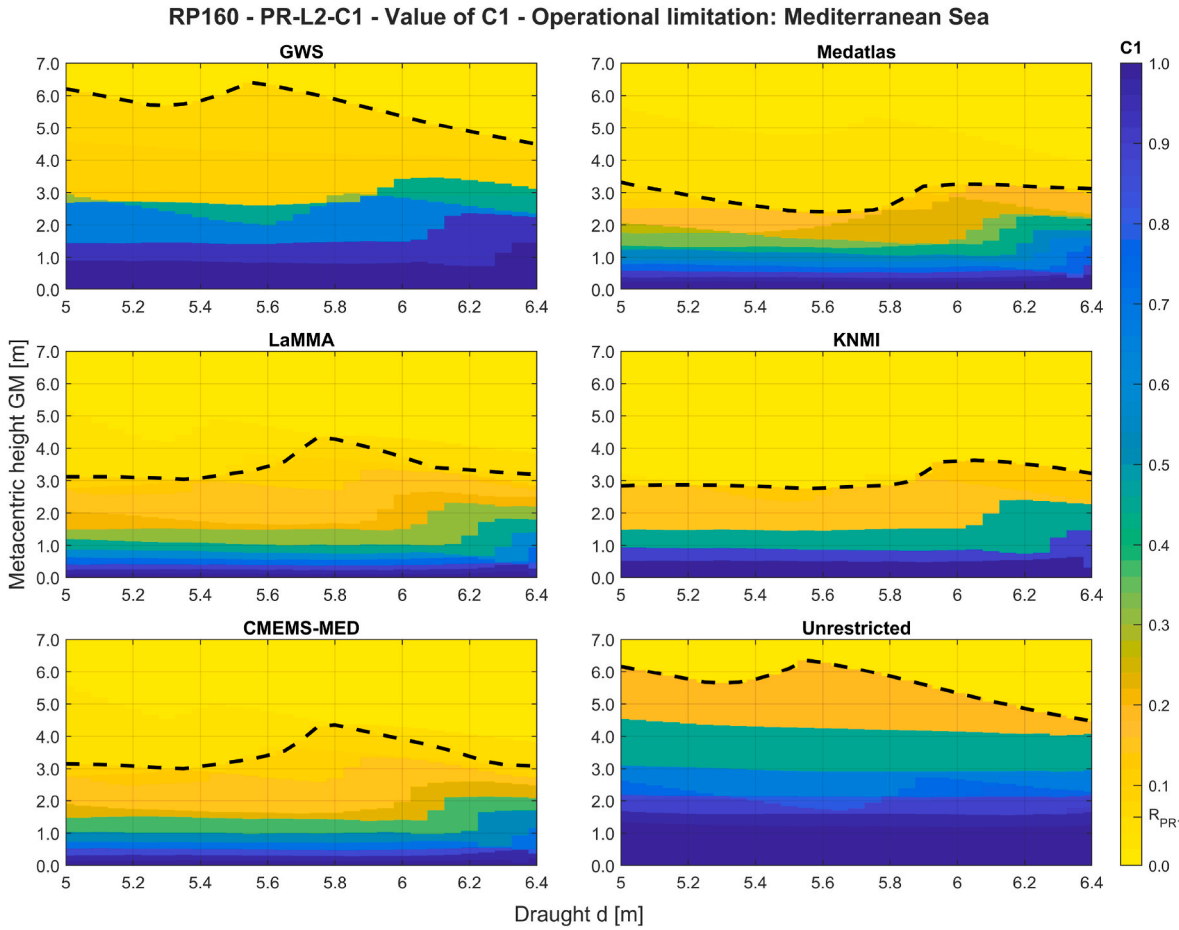

Fig. 12. RP160. Ship without bilge keels. Value of criterion C1 from PR-L2-C1 vulnerability assessment for parametric rolling. Dashed lines represent boundaries between safe and unsafe zones.

Overall, the outcomes from the PR-L1 assessment are such that, for the considered case, a higher level of assessment is necessary in practical applications.

3.3.2. PR-L2-C1 assessment

Fig. 12 and Fig. 13 show the calculated values of C1 from PR-L2-C1 assessment, for the ship without and with bilge keels, respectively. The figures provide results based on wave cases as obtained from the different considered datasets. In addition, results for unrestricted service are also presented. For each case, the identified boundary between safe ($C1 \leq R_{PR1}$) and unsafe ($C1 > R_{PR1}$) regions is reported as a dashed line. Results in Figs. 12 and 13 are based on matrix calculations with a draught discretization of 0.05 m and a *GM* discretization of 0.01 m. Fig. 14 collects the identified boundaries between safe and unsafe zones as obtained from the application of PR-L2-C1 vulnerability assessment for the ship without and with bilge keels. It is noted that the limiting *GM* curve for unrestricted service for the ship without bilge keels is almost coincident with that obtained in case of operational limitations based on GWS dataset.

Compared to the outcomes from PR-L1 assessment, those from PR-L2-C1 assessment in Figs. 12, 13 and 14 provide more realistic limiting metacentric heights. However, also the results of PR-L2-C1 assessment show large differences from a practical perspective, in this case both in absolute value and also regarding the qualitative behaviour of the limiting curve, depending on the source of MetOcean data.

Some qualitative similarities can be observed between outcomes from PR-L2-C1 and PR-L1 assessment. Also in case of PR-L2-C1 assessment, the differences among different sources are larger in case of the vessel without bilge keels (Fig. 14-left) and smaller in case of the vessel equipped with bilge keels (Fig. 14-right). The main reason is to be sought in the fact that, in PR-L2-C1 assessment, the parametric excitation threshold requirement for each wave case (see eq. (3)) depends on the R_{PR} parameter that is used also in PR-L1. In addition, also for PR-L2-C1 assessment, the relative differences are very similar for the configurations with and without bilge keels, and the two sets of limiting curves in Fig. 14 appear to be almost one the scaling of the other.

The dependence of the limiting curves on the draught is not simple, and, although some general trends are common, different sources of MetOcean data lead to different qualitative behaviours.

It is important to note that, while there are some general similarities with the outcomes from PR-L1 assessment, there are important differences. In particular, assuming that some, at least weak/approximate, ordering, in terms of severity, can be introduced in the limiting curves from PR-L2-C1 assessment, such ordering does not correspond, in general, to that obtained, clearly, from PR-L1 assessment. This is particularly evident when looking at results from the use of GWS data, which lead to the least conservative limiting curve in PR-L1 assessment, and to the most conservative curve in case of PR-L2-C1 assessment. This may be, at least partially, a consequence of the already mentioned difficulties in the definition of the wave steepness parameter s_W for PR-L1 assessment from the obtained wave cases from PR-L2-C1 assessment.

Furthermore, a notable characteristic can be observed from the results in Fig. 14. The limiting curves associated with GWS data are the responsible for the very large width of the variability range of limiting *GM*, given draught. Instead, limiting curves based on the other datasets, show a more common behaviour, although differences among them are still large from the point of view of practical application. It is interesting to link this outcome to the fact that GWS data are the only data used in

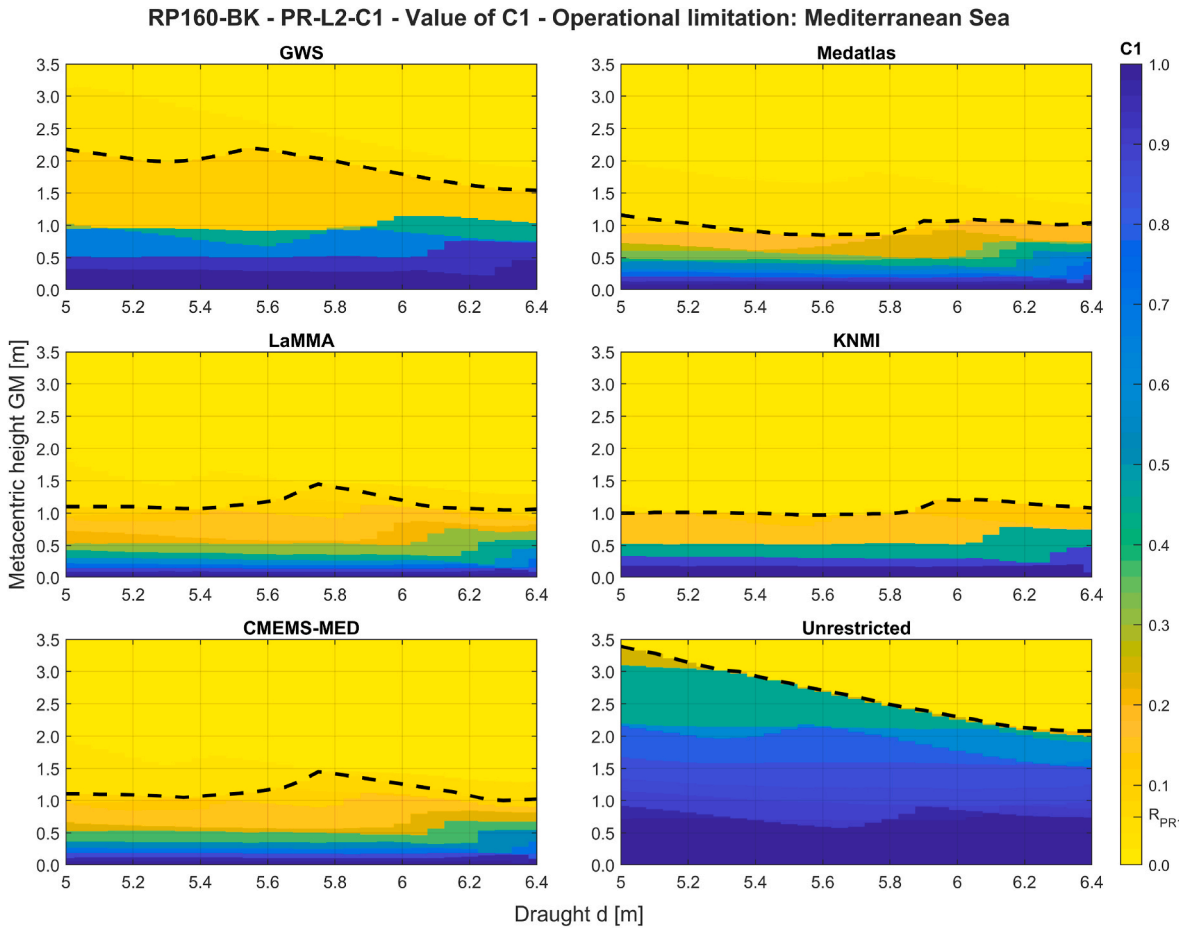

Fig. 13. RP160. Ship with bilge keels. Value of criterion C1 from PR-L2-C1 vulnerability assessment for parametric rolling. Dashed lines represent boundaries between safe and unsafe zones.

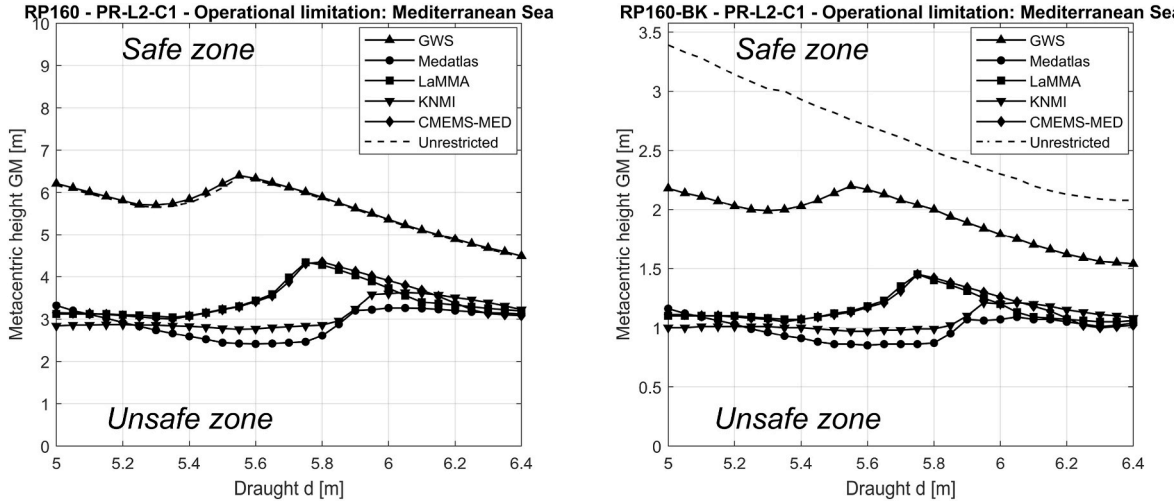

Fig. 14. RP160. Safe zones from PR-L2-C1 vulnerability assessment for parametric rolling. Ship without bilge keels (left) and with bilge keels (right).

this study that are based on visual observations. The other datasets are based, instead, on data from numerical models, with or without calibrations/assimilation, depending on the dataset. At the same time, as already discussed, GWS data are those that are closer to the background of standard environmental conditions presently used in MSC.1/Circ.1627 (IMO, 2020).

Finally, it can also be noted that results obtained under operational limitations generally lead to less stringent limitations on loading conditions compared with those obtained for unrestricted service. The case of vessel without bilge keels and environmental data based on the GWS dataset is an exception, because it provides slightly more conservative limitations in loading conditions compared to results for unrestricted service. Nevertheless, the limiting boundaries are very close, and almost coincident. It is shortly noted here that the obtained picture is essentially opposite to that obtained from PR-L1 assessment, and this point is further discussed hereinafter.

3.4. Additional considerations

3.4.1. Wave steepness factor for PR-L1 assessment

In the presented application example, the determination of the wave steepness factor s_W for PR-L1 assessment proved to be problematic. In fact, it was repeatedly noted in section 3.2 that the maximum wave steepness from PR-L2-C1 wave cases was obtained from the wave case associated with the shortest wave length, where the resolution of the wave scatter tables tend to be insufficient. The result is that wave steepness factors for PR-L1 assessment may be inaccurate and the perception from this example study is that they may be overly conservative.

It is possible that the identified issue is particularly evident in case of Mediterranean Sea, where waves are generally characterised by shorter periods compared to oceanic areas, like, e.g. North Atlantic. However, it cannot be excluded the identified issue to have a potentially more general nature, especially in case of operational areas with environmental characteristics similar to those of the Mediterranean Sea.

From a general perspective, this application study indicates that the definition of the wave steepness for PR-L1 assessment as the maximum steepness from PR-L2-C1 wave case may not represent a very robust approach. In fact, in the PR-L2-C1 assessment, when such large steepness values are associated with short waves, the global effect on the calculations may be limited, because short waves should not generally lead to large variations of stability (this point, however, requires some further comments, which are reported in section 3.4.2 hereinafter). Instead, in PR-L1 assessment, a large steepness value that may occur in short waves from PR-L2-C1 wave cases may be artificially translated, in the limits of the flat waterplanes approximation, to much longer wave lengths, i.e. to a wave length equal to the ship length. This procedure is generally conservative, and therefore it is in principle appropriate for a regulatory framework. However, it may generate artificially and overly large estimated variations of metacentric height in PR-L1 assessment. Furthermore, since, in the analysed example, the maximum wave steepness from PR-L2-C1 wave cases comes from regions where the discretization of the wave scatter tables plays an important role, it is also likely that the identified large wave steepness values are, themselves, somehow artificial.

This is somehow confirmed when comparing results for unrestricted service and results obtained under operational limitations between PR-L1 and PR-L2-C1 assessment. In fact, the results from PR-L2-C1 assessment are essentially opposite to those obtained from PR-L1 assessment. In PR-L1 assessment, unrestricted service results are the least stringent, whereas they are generally the most stringent in case of PR-L2-C1 assessment. Considering the dimension of the example ship, the picture from PR-L2-C1 appears to be more rational compared to what is obtained from PR-L1. This outcome is considered to be a consequence of the fact that PR-L2-C1 assessment better considers the actual distribution of sea states and it is much less affected by the mentioned issues in the region of short waves. Instead, results for PR-L1 assessment are driven by the value of the steepness factor s_W, which, in this case, as discussed, is affected by the mentioned issues in the region of short waves.

In view of the obtained results, it may therefore be advisable to consider possibly more robust approaches for the implementation of operational limitations in PR-L1 assessment.

Investigating such alternative options is out of the scope of this study. Nevertheless, it has been considered hopefully useful to try providing some considerations on possible options to address the identified issue.

Of course one option would be to refine the wave scatter tables in such a way to reduce discretization problems in the region of short waves. However, this approach is directly viable only when raw data are available and when there are enough raw data in the considered region. Furthermore, this approach may be difficult to apply in case the wave scatter table has already been prepared with a given discretization, as this would either require a reanalysis of raw data or a modelling of the

joint distribution of wave period and wave height to support a refinement of the wave scatter table. Eventually, it cannot be excluded that additional refinements may lead to similar issues at further shorter waves.

Another possibility could be to define the wave steepness for PR-L1 by neglecting those wave cases from PR-L2-C1 that are associated with waves that are too short compared to the resolution of the wave scatter table or that are short compared to the ship length. However, implementing such type of "robustifying" constraints could not be straightforward. In fact, it would require to provide a definition of waves that are "too short" compared to the ship length, and such definition should be consistently implemented also in PR-L2-C1 assessment, where "short waves" should be automatically flagged as "non-dangerous" ($C_i = 0$ in the definition of $C1$ index in eq. (2)). Alternatively, or in addition, a definition should also be devised for waves that are "too short" compared to the resolution of the wave scatter table, where "resolution" should be intended both in terms of wave period and significant wave heights. It is nevertheless noted that these concepts may lead to application difficulties in case of relatively small ships that are characterized by limited lengths.

A further option may be to define the wave steepness for PR-L1 assessment abandoning the idea of using the maximum and using, instead, some other relevant, more robust, definition.

For instance, the wave steepness for PR-L1 assessment may be defined as the steepness with a specified probability of exceedance, based on the wave cases used in PR-L2-C1 assessment. A definition based on a given probability of exceedance could in principle reduce the effect of maxima that are essentially outliers, but still some difficulties may remain in practical application, especially in situations with a limited number of wave cases in PR-L2-C1 assessment.

A more empirical, but perhaps more robust definition of s_W for PR-L1 assessment could be based on the multiplication of the average steepness from PR-L2-C1 wave cases by a given factor. Such factor may be tuned, for instance, using the standard condition of unrestricted service. For unrestricted service, the average wave steepness from PR-L2-C1 wave cases can be calculated from Table 2.5.3.2.3 in MSC.1/Circ.1627 (IMO, 2020) as $s_{W,PR,mean} = 0.0162$ (see data in Table 10). The maximum wave steepness from the same PR-L2-C1 wave cases, corresponding to the wave steepness factor for PR-L1 assessment, is $s_W = 0.0167$. Therefore, the ratio for unrestricted service is $s_W/s_{W,PR,mean} = 1.03$. Accordingly, the wave steepness for PR-L1 assessment may be defined as 1.03 times the average wave steepness from PR-L2-C1 wave cases. In case some additional conservativeness would be deemed appropriate in the implementation of operational limitations, such basic reference ratio could be increased.

Of course, in general, any alternative approach for the definition of the wave steepness factor for PR-L1 assessment should be such to provide, at least in the majority of cases, a PR-L1 assessment that is more conservative than the PR-L2 assessment. This should also be properly tested.

Finally, in case the observed difficulties could not be overcome, a drastic, but potentially very effective solution may also be simply not to allow the use of PR-L1 assessment when operational measures are implemented, and to require, in such cases, the use of level 2 or direct stability assessment.

3.4.2. Hydrostatic calculations in short waves

As discussed in section 3.4.1, very short waves introduce difficulties for a proper determination of the corresponding steepness when analysing relevant wave scatter tables. In view of the obtained results, it is worth discussing also an additional point related to short waves, i.e. the topic of hydrostatic calculations in waves that are short compared to the ship dimensions.

As it can be appreciated from the PR-L2-C1 wave cases obtained from the various datasets herein, a number of wave cases have lengths that are short compared to the length of the considered ship. The shorter waves are also short in comparison with the ship draught.

In such cases, the use of hydrostatic calculations in waves may represent a significant simplification due to the lack of consideration of ship-wave interaction (diffraction) effects, and due to the lack of consideration of the non-hydrostatic pressure field. A non-hydrostatic pressure field could be implemented, in principle, but this would lead to non-negligible complications in the calculations. It is therefore important to consider hydrostatic calculations in short waves as indicative practical calculations for relative comparison purposes, and to bear in mind the underlying involved simplifications.

A further aspect related to the consideration of short waves in the calculations, is the discretization of the ship geometry. The shorter the calculation wave, the finer shall be the hull geometry discretization for hydrostatic calculations. Therefore, unless an adaptive hull geometry refinement is implemented, the computational time may be dominated by discretization requirements associated with the shorter waves, where, as discussed, the calculation assumptions may be, to a certain extent, questionable.

The highlighted points indicate that short waves may be associated with some criticalities related to regulatory calculations of initial stability in waves and, more generally, roll restoring in waves. Therefore, it may be useful to address the topic of short waves in some more detail in future investigations.

4. Conclusions

The recently approved Interim Guidelines on the Second Generation Intact Stability Criteria (SGISC), MSC.1/Circ.1627, open the door to a wide application of advanced approaches for intact stability assessment. Considering the novelty of such approaches in the context of a regulatory framework, feedback is expected (see section 1.1.5 in MSC.1/Circ1627), and likely necessary, in the interim application period, as a result of the experience gained in the initial use of the guidelines.

One of the important characteristics of the framework of SGISC is the possibility of embedding non-standard environmental conditions through "operational limitations". Practically, such possibility is implemented through proper modifications of the calculation parameters of the criteria, on the basis of the specifically considered environmental conditions.

The possibility of implementing operational limitations allows, in principle, a more tailored vessel design, taking into account the specific MetOcean conditions that the ship will operate in.

However, MetOcean data are generally available from multiple sources, and different sources provide information on environmental conditions on the basis of different approaches. This leads, in general, to a source-related variability of MetOcean data. This source-related variability basically represents an uncertainty that eventually reflects in an uncertainty in the results of the assessment.

From a regulatory perspective, this uncertainty represents a potential for a reduction in the uniformity of implementation of MSC.1/Circ.1627. Furthermore, the variability in the outcomes of the assessment may lead to opportunistic behaviours in the selection of the MetOcean data that are eventually used for the calculations.

The paper has presented an explorative study aimed at providing an example quantification of how different sources of MetOcean data may affect the outcomes of the stability assessment. The study concentrated on the application of level 1 (PR-L1) and level 2-check 1 (PR-L2-C1) vulnerability assessment criteria for parametric rolling.

A sample RoPax ship has been used as main example case, considering the Mediterranean Sea as operational area. The ship has been considered both without and with bilge keels, to assess their effects on the obtained safe zones and on the variability of outcomes depending on the source of MetOcean data.

Five different sources of MetOcean data have been used for describing the distribution of sea states. Relevant calculation parameters for PR-L1 and PR-L2-C1 have been derived from each source. Among the

five datasets, one dataset is based on visual observations, while the other four datasets are based on numerical modelling with or without calibration/assimilation.

Safe zones of loading conditions have then been determined from the application of PR-L1 and PR-L2-C1 vulnerability assessment criteria for parametric rolling, embedding the considered operational limitation.

The obtained results indicate that, for the considered main example case, the variability in the outcomes of the stability assessment, related to MetOcean data, is large. Such variability is reduced, in absolute terms, when the vessel is assumed to be fitted with bilge keels, but it is still large for practical purposes.

At the same time, it was also observed that the variability in the outcomes reduces when a subset of sources is used. In particular, the variability is reduced when the dataset based on visual observations is excluded.

The reported main application provided also some indications on aspects that would be worth being given further attention.

From the point of view of calculation parameters, wave cases for PR-L2-C1 vulnerability assessment were found to be clearly dependent on the source of MetOcean data. The definition of the calculation steepness for the PR-L1 assessment was governed by the region of short waves, it was clearly sensitive to data processing, and it was significantly dependent on the source of MetOcean data. This indicates that PR-L1 assessment may be associated with a reduced reliability when operational limitations are introduced. In this respect, some possible alternative ways of defining the wave steepness for PR-L1 assessment from the wave cases in the PR-L2-C1 assessment have been outlined and discussed from a general perspective, as starting ideas for possible future investigations. Furthermore, some criticalities have also been highlighted and discussed regarding the consideration of short waves in the determination of initial ship stability and roll restoring in waves.

The application of the PR-L1 criterion resulted in safe zones at metacentric heights that are unrealistically large for the considered main example ship, this requiring the use of a higher level of assessment for practical purposes. The fitting of bilge keels reduced the required metacentric height from the PR-L1 assessment, but requirements were still impractical.

Safe zones of loading conditions from PR-L2-C1 assessment were characterised by more realistic limiting metacentric heights, but the variability related to MetOcean data was found to be still large. Also in case of PR-L2-C1, the fitting of bilge keels led to a reduction in the absolute variability of outcomes from the stability assessment.

Following the same line of investigation as used for the main example case, results for an additional example case using the CEHIPAR2792 hull form have been presented. The additional results essentially confirm the outcomes from the main example case.

The obtained results indicate that the implementation of operational limitations in the framework of SGISC may be linked to a reduced uniformity of application, due to the source-related uncertainty of MetOcean data and due to data processing procedures.

This work concentrated on operational limitations considering vulnerability assessment criteria for parametric rolling. However, the topic of variability and reliability of MetOcean data has a much wider and general impact, encompassing all levels of assessment, when non-standard environmental conditions are considered in “operational measures”, i.e. operational limitations or operational guidance.

Therefore, further work is needed to quantify the effect of MetOcean data uncertainty also in case of stability assessment related to other failure modes and/or levels of assessment. In addition, it is important to devise procedures to promote uniform application also when non-standard environmental conditions are embedded in the stability assessment.

CRediT authorship contribution statement

Gabriele Bulian: Conceptualization, Methodology, Software, Formal analysis, Investigation, Data curation, Writing – original draft, Writing – review & editing, Visualization. **Andrea Orlandi:** Conceptualization, Software, Formal analysis, Resources, Data curation, Writing – review & editing.

Declaration of competing interest

The authors declare that they have no known competing financial interests or personal relationships that could have appeared to influence the work reported in this paper.

Acknowledgements

The authors gratefully acknowledge Dr. Luigi Cavaleri (ISMAR-CNR) for kindly making available the “Wind and Wave Atlas of the Mediterranean Sea – Medatlas”, Dr. Andreas Sterl (KNMI) for the provided information regarding the KNMI/ERA-40 Wave Atlas, and Dr. Frans van Walree (MARIN) for the suggestion of investigating the effect of bilge keels. This study has been partially conducted, and some of the results have been generated, using E.U. Copernicus Marine Service Information.

Appendix

This appendix contains an additional example set of PR-L1 and PR-L2-C1 vulnerability assessment calculations. The scope of this appendix is to provide an additional example application which also allows reproducibility.

To allow reproducibility, calculations have been carried out using the CEHIPAR2792 hull form (Bulian et al., 2009, 2010), which is publicly available. Representative sections of CEHIPAR2792 are shown in Figure A.1, which reports also the design draught. Following the convention reported by Bulian et al. (2009) for CEHIPAR2792, the aft and forward perpendiculars are placed at the aft and forward end, respectively, of the waterline length at the design draught.

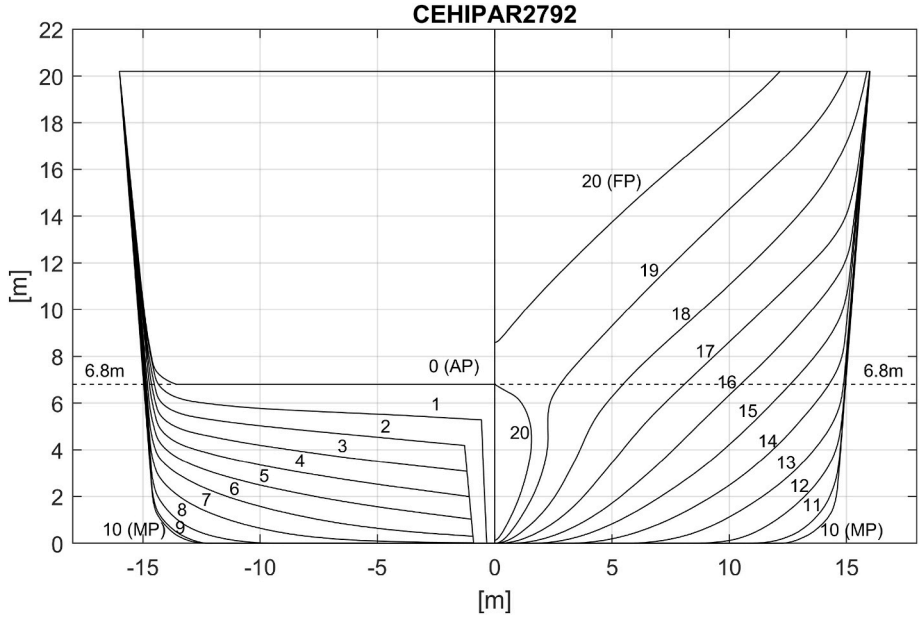

Fig. A.1. CEHIPAR2792. Representative sections.

Since CEHIPAR2792 is a hull form which was intended for research purposes, some data which are necessary for the application of PR-L1 and/or PR-L2-C1 assessment according to MSC.1/Circ.1627 (IMO, 2020) are not available from the original sources. Therefore, some assumptions have been made, as follows:

- The ship length according to MSC.1/Circ.1627 (IMO, 2020) has been approximated by the ship length between perpendiculars as reported by Bulian et al. (2009);
- A reference ship speed for CEHIPAR2792 is not available. Therefore, a notional ship speed of 21 knots has been assumed for the calculations, which corresponds to a Froude number of 0.24 using the reference ship length. This choice was made based on the hull form characteristics and to have a set of example calculations for a ship with significantly different Froude number compared to RP160, which has $Fn = 0.35$ (see data in Table 1).
- The ship breadth has been taken as the breadth of the hull at the maximum depth of the available geometry, and this leads to a breadth of 32 m. Since the ship is characterised by inclined sides (see Figure A.1), this breadth corresponds to the maximum ship breadth and it is larger than the breadth at waterline.
- The ship depth has been taken as the maximum depth of the available geometry, which corresponds to 20.2 m. This is a purely notional value, as the actual depth of a corresponding real ship would be significantly smaller.
- The draught corresponding to the fully loaded departure condition, d_{full}, has been assumed equal to the design draught, i.e. 6.8 m according to Bulian et al. (2009).

The main characteristics for CEHIPAR2792, relevant for the current calculations, are reported in Table A.1. Calculations have been carried out considering only the configuration with bilge keels. The table reports also the value of the R_{PR} coefficient and of the midship section coefficient at d_{full} , i.e. $C_{m.full}$. Since the ship is characterised by inclined sides, it is worth reporting that $C_{m.full}$ has been calculated using the breadth at waterline for the midship section.

Table A.1
CEHIPAR2792. Main characteristics and value of R_{PR} coefficient.

Ship length, L	205.7 m
Ship breadth, B	32 m
Design draught, T	6.8 m
Service speed, V_S	21 knots
Area of bilge keels, A_k	82.2 m^2
Bilge keels area ratio, $A_k/(L \cdot B)$	0.0125
Midship section coefficient, $C_{m.full}$	0.971
R_{PR}	0.7007

Calculations have been carried out for a range of draughts between 5 m and 6.8, with steps of 0.1 m, considering zero trim. For matrix calculations in PR-L2-C1 assessment, the metacentric height was discretized with steps of 0.01 m.

Similarly to RP160, also for CEHIPAR2792 the application of the PR-L2-C1 criterion in the chosen range of draughts and metacentric heights led to the identification of a unique boundary between safe and unsafe regions of loading conditions. Therefore, results for both for PR-L1 and PR-L2-C1 assessment can be presented in terms of limiting curves of metacentric height, in the same way as done for RP160.

Regarding PR-L1 assessment, the calculated values of δGM_1 are shown in Figure A.2, and Figure A.3 shows the curves of limiting metacentric height GM_{min}. Regarding PR-L2-C1 assessment, Figure A.4 shows the calculated values of criterion C1, and Figure A.5 collects the identified boundaries between safe and unsafe zones. To ease comparison between results obtained for CEHIPAR2792 and for RP160, Table A.2 provides a correspondence between respective figures containing the same type of results for the two ships.

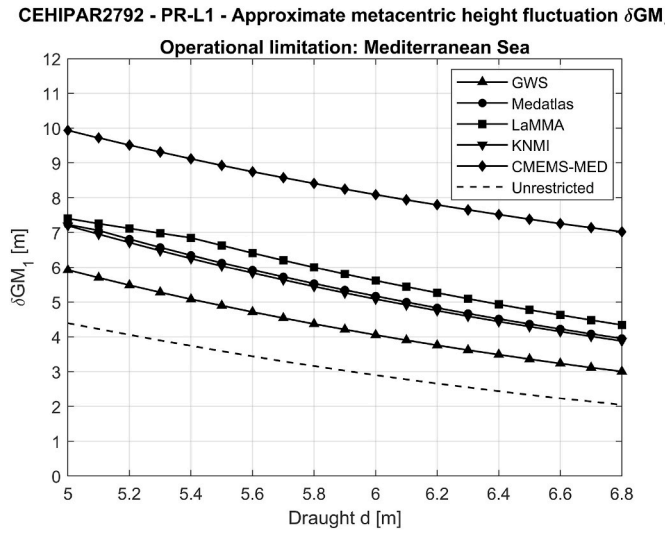

Fig. A.2. CEHIPAR2792. Approximate metacentric height fluctuation, δGM_1.

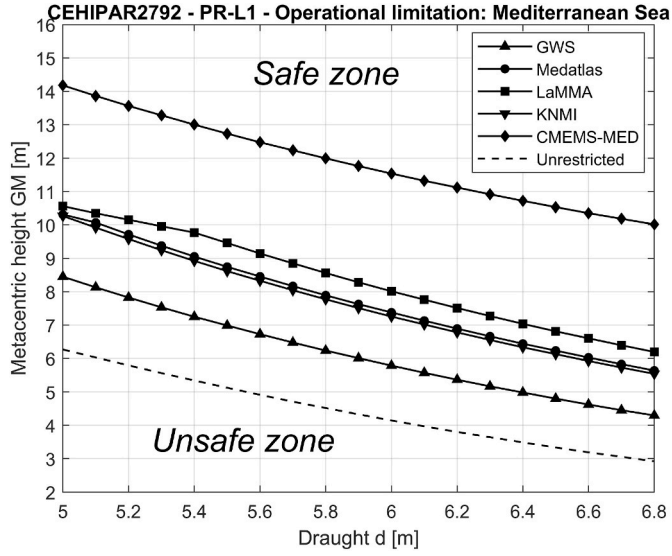

Fig. A.3. CEHIPAR2792. Safe zones from PR-L1 vulnerability assessment for parametric rolling.

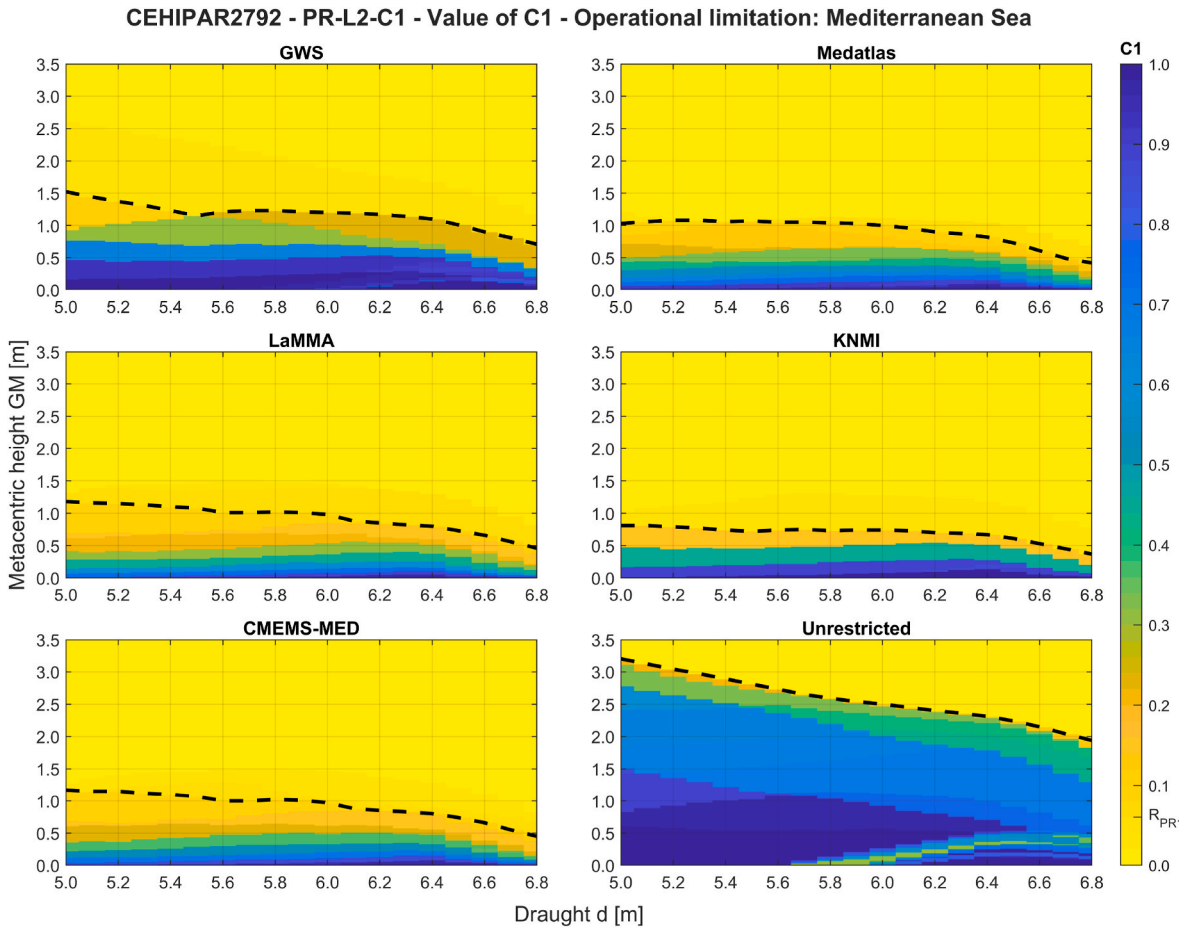

Fig. A.4. CEHIPAR2792. Value of criterion C1 from PR-L2-C1 vulnerability assessment for parametric rolling. Dashed lines represent boundaries between safe and unsafe zones.

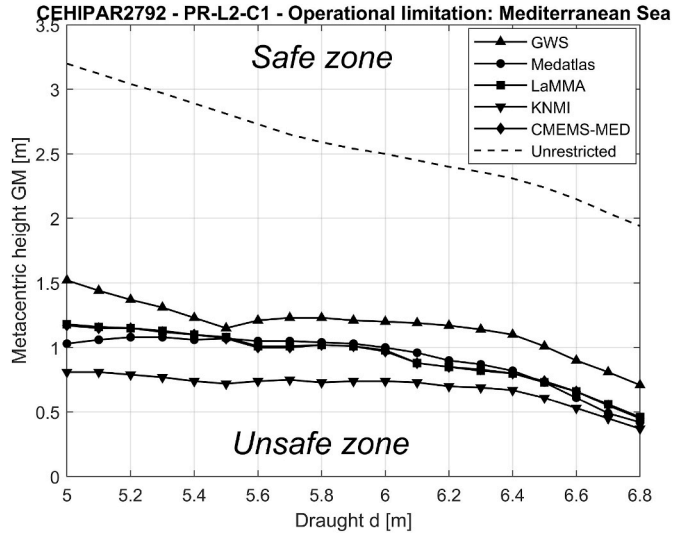

Fig. A.5. CEHIPAR2792. Safe zones from PR-L2-C1 vulnerability assessment for parametric rolling.

Table A.2
Correspondence of figures for comparison of results between CEHIPAR2792 and RP160.

CEHIPAR2792	RP160(-BK)
Figure A.2	Fig. 10
Figure A.3	Fig. 11
Figure A.4	Figs. 12 and 13
Figure A.5	Fig. 14

Results regarding PR-L1 assessment for CEHIPAR2792 qualitatively show the same behaviors observed for RP160 (compare Figure A.2 to Fig. 10, and Figure A.3 to Fig. 11). Therefore, essentially the same considerations provided for the case of RP160 apply also for CEHIPAR2792. A large variability depending on the source of data is observed due to the different values of the steepness factor s_W, and results for unrestricted service are associated with the smallest limiting metacentric height.

Results regarding PR-L2-C1 in Figure A.4 and Figure A.5 show a quite large variability in the curves of limiting metacentric heights, depending on the source of environmental data. In contrast to the results from PR-L1 assessment (see Figure A.3), PR-L2-C1 results obtained under the considered operational limitations (see Figure A.5) generally lead to less stringent limitations on loading conditions compared with those obtained for unrestricted service. The results obtained for CEHIPAR2792 show similarities with those obtained for RP160 (compare, in particular, Figure A.5 with Fig. 14), although the limiting curves for the two ships show more diversified behaviours. It is notable that the variability of limiting curves for CEHIPAR2792 in Figure A.5 is governed by results based on GWS and KNMI datasets. Limiting curves based on Medatlas, LaMMA and CMEMS-MED datasets are, instead, very close each other. In particular, limiting curves based on LaMMA and CMEMS-MED datasets are almost coincident, and this characteristic resembles results obtained for RP160 (see Fig. 14).

References

Athanassoulis, G.A., Stefanakos, Ch.N., Gerostathis, Th.P., Gaillard, P., Ravazzola, P., Kontolios, Ch., Cavaleri, L., Bertotti, L., Sclavo, M., Ramieri, E., Dentone, L., Noel, C., Viala, C., Lefèvre, J.-M., 2004a. Wind and Wave Atlas of the Mediterranean Sea. Western European Union, Western European Armaments Organisation Research Cell, April.

Athanassoulis, G., Stefanakos, Ch., Cavaleri, L., Ramieri, E., Noël, C., Lefevre, J.M., Gaillard, P., 2004b. RTP 10.10/WW_MEDATLAS – Scientific Report. 14 April.

Bačkalov, I., Bulian, G., Rosén, A., Shigunov, V., Themelis, N., 2016. Improvement of ship stability and safety in intact condition through operational measures: challenges and opportunities. Ocean Eng. 120, 353–361. https://doi.org/10.1016/j.oceaneng.2016.02.011.

Baordo, F., Clementi, E., Iovino, D., Masina, S., 2020. Intercomparison and assessment of wave models at global scale. CMCC Techn. Notes TN0287 (May), 1–49.

Bhaskaran, P.K., 2019. Challenges and future directions in ocean wave modeling - A review. J. Extr. Events 06 (02), 1950004. https://doi.org/10.1142/S2345737619500040, 1-40.

Bitner-Gregersen, E.M., Ewans, K., Johnson, M.C., 2014. Some uncertainties associated with wind and wave description and their importance for engineering applications. Ocean Eng. 86, 11–25. https://doi.org/10.1016/j.oceaneng.2014.05.002.

BMT, 2021. Global Wave Statistics Online. https://www.globalwavestatisticsonline.com. (Accessed 24 October 2021).

Bulian, G., Francescutto, A., Fucile, F., 2009. Determination of Relevant Parameters for the Alternative Assessment of Intact Stability Weather Criterion on Experimental Basis. EU-Funded Project HYD-III-CEH-5 (Integrated Infrastructure Initiative HYDRALAB III, Contract No. 022441 (RII3)). University of Trieste. , 22 November. Report and ship geometry available from: www.shipstab.org.

Bulian, G., Francescutto, A., Fucile, F., 2010. An experimental investigation in the framework of the alternative assessment for the IMO weather criterion. In: Proc. Hydralab III Joint Transnational Access User Meeting, Hannover, February, pp. 251–254.

Bulian, G., Francescutto, A., 2021. An approach for the implementation of operational limitations in the level 1 vulnerability criterion for the dead ship condition. In: Proc. 1st International Conference on the Stability and Safety of Ships and Ocean Vehicles (STAB&S2021), 7-11 June, Online Conference Organised by University of Strathclyde. Glasgow, Scotland, UK. Paper IS1.

Bulian, G., Orlandi, A., 2021. Operational measures in second generation intact stability criteria: effect of source of environmental data. In: Proc. 1st International Conference on the Stability and Safety of Ships and Ocean Vehicles (STAB&S2021), 7-11 June, Online Conference Organised by University of Strathclyde. Glasgow, Scotland, UK. Paper OS7.

Caires, S., Sterl, A., 2005. A new nonparametric method to correct model data: application to significant wave height from the ERA-40 Re-Analysis. J. Atmos. Ocean. Technol. 22 (4), 443–459. https://doi.org/10.1175/JTECH1707.1.

Campos, R.M., Guedes Soares, C., 2016. Comparison and assessment of three wave hindcasts in the North Atlantic Ocean. J. Operat. Oceanogr. 9 (1), 26–44. https://doi.org/10.1080/1755876X.2016.1200249.

Cao, D., Tolman, H.L., Chen, H.S., Chawla, A., Gerald, V.M., 2009. Performance of the ocean wave ensemble forecast system at NCEP. In: MMAB Contribution Nr. 279 and Proc. 11th International Workshop on Wave Hindcasting and Forecasting and Coastal Hazard Symposium, 18-23 October, Halifax, Canada, 12p.

Cavaleri, L., 2005. The wind and wave atlas of the Mediterranean Sea – the calibration phase. Adv. Geosci. 2, 255–257.

Cavaleri, L., Alves, J.-H.G.M., Ardhuin, F., Babanin, A., Banner, M., Belibassakis, K., Benoit, M., Donelan, M., Groeneweg, J., Herbers, T.H.C., Hwang, P., Janssen, P.A.E.M., Janssen, T., Lavrenov, I.V., Magne, R., Monbaliu, J., Onorato, M., Polnikov, V., Resio, D., Rogers, W.E., Sheremet, A., McKee Smith, J., Tolman, H.L., van Vledder, G., Wolf, J., Young, I., 2007. Wave modelling – The state of the art. Prog. Oceanogr. 75 (4), 603–674.

Cavaleri, L., Barbariol, F., Benetazzo, A., 2020. Wind-wave modeling: where we are, where to go. J. Mar. Sci. Eng. 8 (260), 1–15.

Chu, P.C., Miller, S.E., Hansen, J.A., 2015. Fuel-saving ship route using the Navy's ensemble meteorological and oceanic forecasts. J. Defense Model. Simulat. 12 (1), 41–56. https://doi.org/10.1177/1548512913516552.

CMEMS, 2021. Copernicus Marine Service. https://marine.copernicus.eu/. (Accessed 24 October 2021).

de Hauteclocque, G., Zhu, T., Johnson, M., Austefjord, H., Bitner-Gregersen, E., 2020. Assessment of global wave datasets for long term response of ships. In: Proc. 39th International Conference on Ocean, Offshore and Arctic Engineering (OMAE 2020), June 28-July 3, Fort Lauderdale, USA paper OMAE2020/18874.

ECMWF, 2021. ERA5. https://www.ecmwf.int/en/forecasts/datasets/reanalysis-datasets/era5. (Accessed 24 October 2021).

GFS, 2021. Global Forecast System (GFS). www.ncdc.noaa.gov/data-access/model-data/model-datasets/global-forcast-system-gfs. (Accessed 24 October 2021).

Guedes Soares, C., 1999. On the uncertainty in long-term predictions of wave induced loads on ships. Mar. Struct. 12, 171–182.

Hashimoto, H., Taniguchi, Y., Fujii, M., 2017. A case study on operational limitations by means of navigation simulation. In: Proc. 16th International Ship Stability Workshop (ISSW 2017), 5-7 June, Belgrade, Serbia, pp. 41–48.

Hashimoto, H., Furusho, K., 2021. Application of operational limitations to the parametric rolling failure mode. In: Proc. 1st International Conference on the Stability and Safety of Ships and Ocean Vehicles (STAB&S2021), 7-11 June, Online Conference Organised by University of Strathclyde, Glasgow, Scotland, UK. Paper OS13.

Hinnenthal, J., Clauss, G., 2010. Robust Pareto-optimum routing of ships utilising deterministic and ensemble weather forecasts. Ships Offshore Struct. 5 (2), 105–114. https://doi.org/10.1080/17445300903210988.

Hoffschildt, M., Bidlot, J.-R., Hansen, B., Janssen, P.A.E.M., 1999. Potential benefit of ensemble forecasts for ship routing. ECMWF Technical Memorandum Nr. 287, 25p. https://doi.org/10.21957/10.21957/ucgxanos0.

IACS, 2001. Recommendation No.34 – Standard Wave Data (Corr. Nov. 2001). International Association of Classification Societies.

IMO, 2019. SDC 7/INF.2 – Information Collected by the Correspondence Group on Intact Stability. 26 November. Submitted by Japan.

IMO, 2020. MSC.1/Circ.1627 - Interim Guidelines for the Second Generation Intact Stability Criteria. 10 December.

IMO, 2021a. International Code on Intact Stability, 2008 – as Amended, Consolidated edition.

IMO, 2021b. Documents SDC 8/5,Add.1-6 - Development of Explanatory Notes to the Interim Guidelines on Second Generation Intact Stability Criteria - Report of the Correspondence Group (Part 1 to 7). Submitted by Japan, 4 October.

Janssen, P., 2002. The wave model - May 1995. Meteorological Training Course Lecture Series, Education Material. ECMWF. https://www.ecmwf.int/node/16951.

Kalnay, E., 2003. Atmospheric Modeling, Data Assimilation and Predictability. Cambridge University Press.

Komen, G.J., Cavaleri, L., Donelan, M., Hasselmann, K., Hasselmann, S., Janssen, P., 1994. Dynamics and Modelling of Ocean Waves. Cambridge University Press.

Korres, G., Ravdas, M., Zacharioudaki, A., 2019. Mediterranean Sea Waves Hindcast (CMEMS MED-Waves) [Data Set]. Copernicus Monitoring Environment Marine Service (CMEMS). https://doi.org/10.25423/CMCC/MEDSEA_HINDCAST_WAV_006_012.

Korres, G., Ravdas, M., Zacharioudaki, A., Sotiropoulou, M., Denaxa, D., Lecci, R., 2021. Product User Manual for Mediterranean Sea Waves Reanalysis Product MEDSEA_MUTLIYEAR_WAV_006_012 (CMEMS-MED-PUM-006-012). Issue 2.0. Copernicus Marine Environment Monitoring Service. , January.

Krata, P., Szlapczynska, J., 2018. Ship weather routing optimization with dynamic constraints based on reliable synchronous roll prediction. Ocean Eng. 150, 124–137. https://doi.org/10.1016/j.oceaneng.2017.12.049.

Kuhlemann, S., Tierney, K., 2020. A genetic algorithm for finding realistic sea routes considering the weather. J. Heuristics 26, 801–825. https://doi.org/10.1007/s10732-020-09449-7.

Lionello, P., Günther, H., Janssen, P.A.E.M., 1992. Assimilation of altimeter data in a global third-generation wave model. J. Geophys. Res. 97 (C9), 14453–14474. https://doi.org/10.1029/92JC01055.

Ludeno, G., Orlandi, A., Lugni, C., Brandini, C., Soldovieri, F., Serafino, F., 2014. X-band marine radar system for high-speed navigation purposes: a test case on a Cruise ship. Geosci. Rem. Sens. Lett. IEEE 11 (1), 244–248. https://doi.org/10.1109/LGRS.2013.2254464.

Maki, A., Akimoto, Y., Nagata, Y., Kobayashi, S., Kobayashi, E., Shiotani, S., Ohsawa, T., Umeda, N., 2011. A new weather-routing system that accounts for ship stability based on a real-coded genetic algorithm. J. Mar. Sci. Technol. 16, 311–322. https://doi.org/10.1007/s00773-011-0128-z.

Manderbacka, T., 2019. On the uncertainties of the weather routing and support system against dangerous conditions. In: Proc. 17th International Ship Stability Workshop (ISSW 2019), Helsinki, Finland, pp. 221–226.

Meucci, A., Young, I.R., Breivik, Ø., 2018. Wind and wave extremes from atmosphere and wave model ensembles. J. Clim. 31 (21), 8819–8842. https://doi.org/10.1175/JCLI-D-18-0217.1.

Mezaoui, B., Shoji, R., Tamaru, H., Nishiyama, H., 2012. A study on the use of ensemble weather forecasts for ship's weather routeing. J. Jpn. Inst. Navig. 126, 265–275. https://doi.org/10.9749/jin.126.265.

Milliff, R.F., Bonazzi, A., Wikle, C.K., Pinardi, N., Berliner, L.M., 2011. Ocean ensemble forecasting. Part I: ensemble Mediterranean winds from a Bayesian hierarchical model. Q. J. R. Meteorol. Soc. 137 (657), 858–878. https://doi.org/10.1002/qj.767.

Nielsen, U.D., 2021. Spatio-temporal variation in sea state parameters along virtual ship route paths. J. Operat. Oceanogr. https://doi.org/10.1080/1755876X.2021.1872894. Online First, 1-18.

Orlandi, A., Pasi, F., Onorato, L.F., Gallino, S., 2008. An observational and numerical case study of a flash sea storm over the Gulf of Genoa. Adv. Sci. Res. 2, 107–112.

Orlandi, A., Brandini, C., Pasi, F., Taddei, S., Doronzo, B., Brugnoni, G., Rossini, G., Benedetti, R., Gozzini, B., Ortolani, A., Vaccari, F.P., 2011. Implementation of a meteo-marine forecasting chain and comparison between modeled and observed data in the Ligurian and Tyrrhenian seas. In: Marine Research at CNR, Edition: DTA/06-2011. Publisher: National Research Council of Italy, Department of Earth and Environment, pp. 2301–2313.

Orlandi, A., Bruzzone, D., 2011. Numerical weather and wave prediction models for weather routing, operation planning and ship design: The relevance of multimodal wave spectra. In: Sustainable Maritime Transportation and Exploitation of Sea Resources - Proceedings of the 14th International Congress of the International Maritime Association of the Mediterranean (IMAM 2011), 13-16 September 2011, Genoa, Italy. CRC Press, Taylor & Francis Group, London, UK, pp. 817–826.

Orlandi, A., Pasi, F., Capecchi, V., Coraddu, A., Villa, D., 2015. Powering and seakeeping forecasting for energy efficiency: assessment of the fuel savings potential for weather routing by in-service data and ensemble prediction techniques. In: Towards Green Marine Technology and Transport – Proceedings of the 16th International Congress of the International Maritime Association of the Mediterranean (IMAM 2015), 21-24 September 2015, Pula, Croatia. CRC Press, Taylor & Francis Group, pp. 31–42.

Orlandi, A., Guarnieri, F., Busillo, C., Calastrini, F., Coraddu, A., 2018. Air quality simulations and forecasting of along-route ship emissions in realistic meteo-marine scenarios. In: Technology and Science for the Ships of the Future - Proceedings of NAV 2018: 19th International Conference on Ship and Maritime Research, 20–22 June 2018. IOS Press, Trieste, Italy, pp. 452–461. https://doi.org/10.3233/978-1-61499-870-9-452.

Orlandi, A., Cappugi, A., Mari, R., Pasi, F., Ortolani, A., 2021. Meteorological navigation by integrating Metocean forecast data and ship performance models into an ECDIS-like e-navigation prototype interface. J. Mar. Sci. Eng. 9 (502), 1–29.

Osinski, R.D., Radtke, H., 2020. Ensemble hindcasting of wind and wave conditions with WRF and WAVEWATCH III® driven by ERA5. Ocean Sci. 16 (2), 355–371. https://doi.org/10.5194/os-16-355-2020.

Park, J., Kim, N., 2015. Two-phase approach to optimal weather routing using geometric programming. J. Mar. Sci. Technol. 20, 679–688. https://doi.org/10.1007/s00773-015-0321-6.

Paroka, D., Muhammad, A.H., Rahman, S., 2021. Excessive acceleration criterion applied to an Indonesia Ro-Ro ferry. In: Proc. 1st International Conference on the Stability and Safety of Ships and Ocean Vehicles (STAB&S2021), 7-11 June, Online Conference Organised by University of Strathclyde, Glasgow, Scotland, UK. Paper IS14.

Pasi, F., Orlandi, A., Onorato, L.F., Gallino, S., 2011. A study of the 1 and 2 January 2010 sea-storm in the Ligurian sea. Adv. Sci. Res. 6, 109–115.

Petacco, N., Gualeni, P., 2020. IMO Second Generation Intact Stability criteria: General overview and focus on operational measures. J. Mar. Sci. Eng. 8 (494), 1–20.

Petacco, N., Gualeni, P., 2021. An overview about operational measures in the framework of Second Generation Intact Stability criteria. In: Proc. 1st International Conference on the Stability and Safety of Ships and Ocean Vehicles (STAB&S2021), 7-11 June, Online Conference Organised by University of Strathclyde, Glasgow, Scotland, UK. Paper IS5.

Pinardi, N., Bonazzi, A., Dobricic, S., Milliff, R.F., Wikle, C.K., Berliner, L.M., 2011. Ocean ensemble forecasting. Part II: Mediterranean Forecast System response. Q. J. R. Meteorol. Soc. 137 (657), 879–893. https://doi.org/10.1002/qj.816.

Rinauro, B., Begovic, E., Gatin, I., Jasak, H., 2020. Surf-riding operational measures for fast semidisplacement naval hull form. In: Proc. 12th Symposium on High Speed Marine Vehicles (HSMV 2020), 15-16 October, Napoli/Online, pp. 219–228.

Rudaković, S., Bačkalov, I., 2019. Operational limitations of a river-sea container vessel in the framework of the Second Generation Intact Stability Criteria. Ocean Eng. 183, 409–418. https://doi.org/10.1016/j.oceaneng.2019.05.013.

Saetra, Ø., Bidlot, J.-R., 2002. Assessment of the ECMWF ensemble prediction system for waves and marine winds. ECMWF Technical Memorandum Nr. 388, 29p. https://doi.org/10.21957/68qw9y7e0.

Sasdelli, M., 2015. IMO Second Generation Intact Stability Criteria: A Case Study on Parametric Roll Assessment for a Containership. M.Sc. Thesis. University of Trieste, Italy,. Academic Year 2014-2015.

Schirmann, M.L., Collette, M.D., Gose, J.W., 2020. Significance of wave data source selection for vessel response prediction and fatigue damage estimation. Ocean Eng. 216, 107610 https://doi.org/10.1016/j.oceaneng.2020.107610, 1-15.

Shigunov, V., Themelis, N., Bačkalov, I., Begovic, E., Eliopoulou, E., Hashimoto, H., Hinz, T., McCue, L., Míguez González, M., Rodríguez, C.A., 2021. Operational measures for intact ship stability. In: Proc. 1st International Conference on the Stability and Safety of Ships and Ocean Vehicles (STAB&S2021), 7-11 June, Online Conference Organised by University of Strathclyde, Glasgow, Scotland, UK. Paper OS5.

Skoglund, L., Kuttenkeuler, J., Rosén, A., Ovegård, E., 2015. A comparative study of deterministic and ensemble weather forecasts for weather routing. J. Mar. Sci. Technol. 20, 429–441. https://doi.org/10.1007/s00773-014-0295-9.

Sterl, A., Caires, S., 2006. Climatology, variability and extrema of ocean waves – The web-based KNMI/ERA-40 wave atlas. In: Proc. 25th International Conference on Offshore Mechanics and Arctic Engineering (OMAE2006), June 4-9, Hamburg, Germany paper OMAE2006-92568.

Stopa, J.E., Ardhuin, F., Babanin, A., Zieger, S., 2016. Comparison and validation of physical wave parameterizations in spectral wave models. Ocean Model. 103, 2–17.

Szlapczynska, J., Szlapczynski, R., 2019. Preference-based evolutionary multi-objective optimization in ship weather routing. Appl. Soft Comput. J. 84, 105742 https://doi.org/10.1016/j.asoc.2019.105742.

The WAMDI Group, 1988. The WAM Model - A Third Generation Ocean Wave Prediction Model. J. Phys. Oceanogr. 18 (12), 1775–1810. https://doi.org/10.1175/1520-0485(1988)018<1775:TWMTGO>2.0.CO;2.

Uppala, S.M., KÅllberg, P.W., Simmons, A.J., Andrae, U., Bechtold, V.D.C., Fiorino, M., Gibson, J.K., Haseler, J., Hernandez, A., Kelly, G.A., Li, X., Onogi, K., Saarinen, S., Sokka, N., Allan, R.P., Andersson, E., Arpe, K., Balmaseda, M.A., Beljaars, A.C.M., Berg, L.V.D., Bidlot, J., Bormann, N., Caires, S., Chevallier, F., Dethof, A., Dragosavac, M., Fisher, M., Fuentes, M., Hagemann, S., Hólm, E., Hoskins, B.J., Isaksen, L., Janssen, P.a.E.M., Jenne, R., Mcnally, A.P., Mahfouf, J.-F., Morcrette, J.-J., Rayner, N.A., Saunders, R.W., Simon, P., Sterl, A., Trenberth, K.E., Untch, A., Vasiljevic, D., Viterbo, P., Woollen, J., 2005. The ERA-40 re-analysis. Q. J. R. Meteorol. Soc. 131, 2961–3012. https://doi.org/10.1256/qj.04.176.

Vettor, R., Szlapczynska, J., Szlapczynski, R., Tycholiz, W., Guedes Soares, C., 2020. Towards improving optimised ship weather routing. Pol. Marit. Res. 27 (1), 60–69. https://doi.org/10.2478/pomr-2020-0007.

WW3, 2021. WAVEWATCH III®. https://polar.ncep.noaa.gov/waves/wavewatch. (Accessed 24 October 2021).

WRF, 2021. Weather Research And Forecasting (WRF) Model. https://www.mmm.ucar.edu/weather-research-and-forecasting-model. (Accessed 24 October 2021).

Zacharioudaki, A., Ravdas, M., Korres, G., Lyubartsev, V., 2020. Mediterranean Production Centre - MEDSEA_MUTLIYEAR_WAV_006_012 - Quality Information Document (CMEMS-MED-QUID-006-012). Issue 2.0, 15 January. Copernicus Marine Environment Monitoring Service (CMEMS).